iScience

Article

Integrating complementary approaches reveals antigen-reactive CD4$^+$ T cell states after SARS-CoV-2 vaccination

Graphical abstract

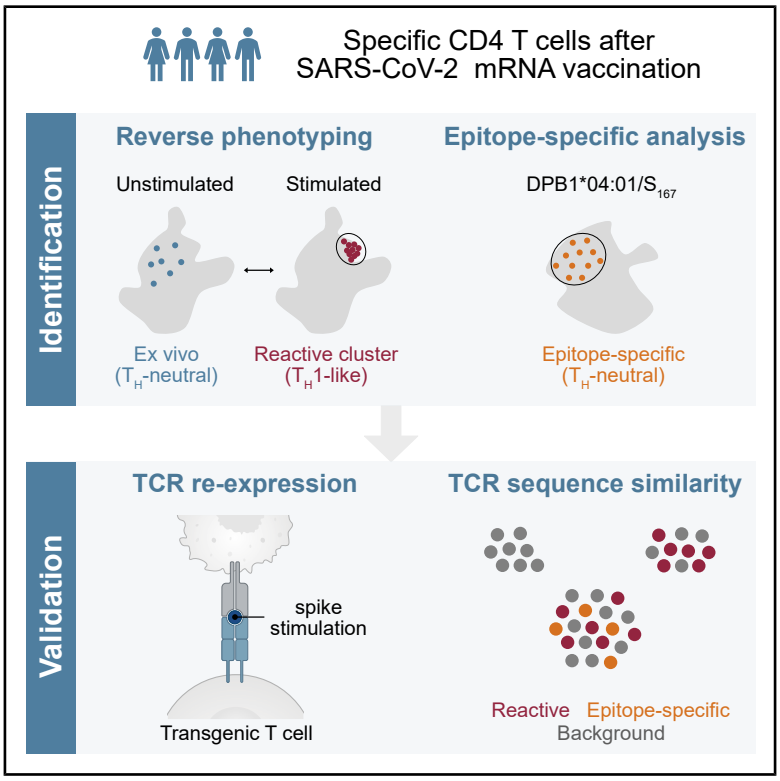

Highlights

- Different methods reveal complementary states of antigen-reactive CD4$^+$ T cells
- Reactive clones are Th-neutral at rest but Th1-like after stimulation
- TCR re-expression separates antigen-specific from bystander clones

Authors

Katharina Kocher, Felix Drost, Christine Schülein, Bernd Spriewald, Benjamin Schubert, Kilian Schober

Correspondence

kilian.schober@uk-erlangen.de

In brief

Therapeutics; Immunology; Virology

Kocher et al., 2026, iScience *29*, 116175
June 19, 2026
https://doi.org/10.1016/j.isci.2026.116175

CellPress

iScience

CellPress
OPEN ACCESS

Article

Integrating complementary approaches reveals antigen-reactive CD4$^+$ T cell states after SARS-CoV-2 vaccination

Katharina Kocher,[1,2,7] Felix Drost,[3,4,7] Christine Schülein,[1] Bernd Spriewald,[5] Benjamin Schubert,[3] and Kilian Schober[1,6,8,*]

[1]Mikrobiologisches Institut – Klinische Mikrobiologie, Immunologie und Hygiene, Universitätsklinikum Erlangen und Friedrich-Alexander-Universität (FAU) Erlangen-Nürnberg, Erlangen, Germany
[2]Division of Infection and Immunity, University College London, London, UK
[3]Institute of Computational Biology, Helmholtz Zentrum München – German Research Center for Environmental Health, Neuherberg, Germany
[4]School of Life Sciences Weihenstephan, Technical University of Munich, Munich, Germany
[5]Department of Internal Medicine 5, Universitätsklinikum Erlangen and Friedrich-Alexander-Universität (FAU) Erlangen-Nürnberg, Erlangen, Germany
[6]FAU Profile Center Immunomedicine, FAU Erlangen-Nürnberg, Erlangen, Germany
[7]These authors contributed equally
[8]Lead contact
*Correspondence: kilian.schober@uk-erlangen.de
https://doi.org/10.1016/j.isci.2026.116175

SUMMARY

Understanding antigen reactivity is crucial for characterizing CD4$^+$ T helper (Th) cell fate, yet conventional peptide restimulation assays introduce phenotypic bias by activating cells *ex vivo*. By combining single-cell RNA and T cell receptor (TCR) sequencing on antigen-stimulated and unstimulated samples, clonotypes can be tracked across conditions to identify antigen-reactive CD4$^+$ T cells while assessing their phenotypes in the unperturbed state. Using this "reverse phenotyping" strategy, complemented by DNA-barcoded peptide-HLA class II multimers and TCR similarity metrics, we tracked SARS-CoV-2 spike-reactive CD4$^+$ T cells longitudinally after repeated mRNA vaccination. Without stimulation, reactive clones showed more Th-neutral features and less activated Th1-like states than after restimulation. Furthermore, transgenic TCR re-expression further separated antigen-specific from bystander-activated clones. These results demonstrate the complementary value of different methods to identify and characterize antigen-reactive CD4$^+$ T cells, and highlight that cell state classification can differ when defined by phenotype versus function.

INTRODUCTION

The fate of a T cell is determined by the specific antigen it recognizes. Accurately identifying antigen-reactive T cells is crucial for understanding immune responses, yet most available methods rely on *ex vivo* stimulation followed by the detection of activation markers or cytokines.[1] While these assays are effective for detecting functional reactivity, they can alter the cells' native phenotype[2] and may inadvertently include cells that are activated independently of antigen specificity, known as bystander-activated cells.[3] Therefore, there is a pressing need for approaches that can identify antigen-reactive T cells without introducing such stimulation-induced phenotypic bias. This challenge is particularly pronounced for CD4$^+$ T cells, as generating peptide-human leukocyte antigen (pHLA) multimers for HLA class II is more complex than for class I.

Nevertheless, for pathogens such as SARS-CoV-2, many immunodominant HLA class II-restricted epitopes have been characterized,[4–11] such as DPB1*04:01/S_{167}, DRB1*15:01/S_{751}, S_{816} (potentially presented by multiple HLA alleles), and DRB1*15:01/S_{870}. For some of these epitopes, pHLA class II multimers are available and have been instrumental in characterizing the phenotype of SARS-CoV-2 epitope-specific CD4$^+$ T cells, especially in settings with limited cell numbers *ex vivo*.[8,12] However, pHLA class II multimers are inherently restricted to the analysis of individual epitopes, limiting their ability to provide a comprehensive view of antigen reactivity that broader antigen restimulation approaches can offer. To address these limitations, we previously demonstrated that it is possible to combine the strengths of both strategies by tracking how a T cell clone responds to antigenic stimulation and retrospectively examining its phenotype in the unstimulated state.[13] We termed this method "reverse phenotyping." Our initial proof-of-concept study, however, was constrained by non-standardized samples collected at varying time points during or after severe COVID-19 infection.[13] Despite these constraints, we corroborated earlier findings of a cytotoxic Th1 (type 1 helper T cell) lineage-driven response of CD4$^+$ T cells to SARS-CoV-2 infection.[14–18]

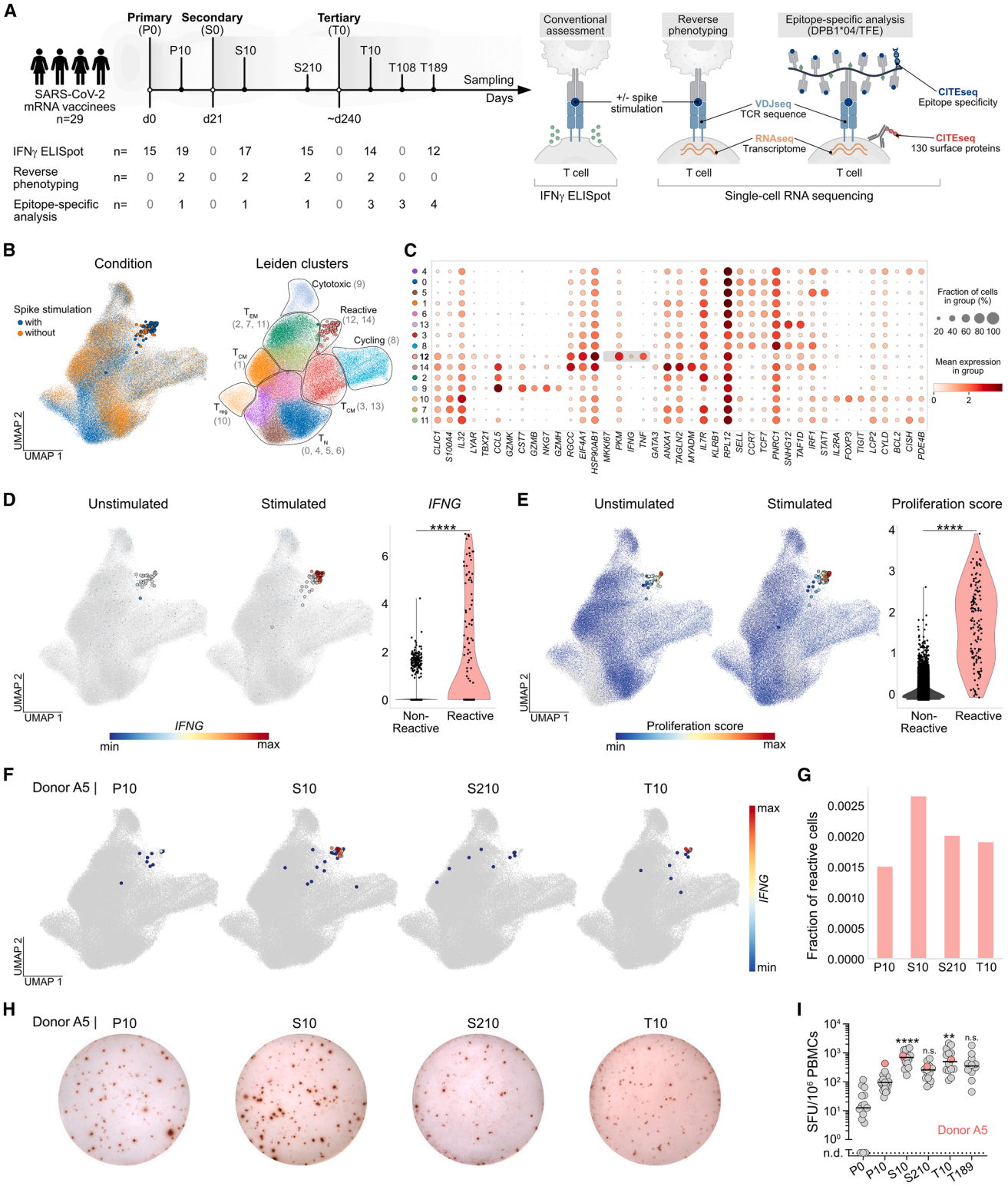

Figure 1. Identification of SARS-CoV-2-specific T cell responses by reverse phenotyping

(A) CoVa-Adapt study design and sample collection scheme. For all donors, PBMCs were collected at day 0 (P0), 10 days after primary (P10), 10 and 210 days after secondary (S10, S210), and 10 and 189 days after tertiary (T10, T189) vaccination. For selected donors, PBMCs were additionally sampled 108 days after tertiary vaccination (T108, *n* = 7). Vaccination-induced T cell responses were characterized for most donors on a quantitative level by IFNγ ELISpot. Selected

(legend continued on next page)

Importantly, reverse phenotyping revealed that transcriptional signatures of "Th1-ness" (as indicated by the expression of the hallmark transcription factor *TBX21*) are overestimated following *ex vivo* peptide stimulation (or, in fact, underestimated without stimulation).[13] While this does not negate the Th1 and cTfh predominance in blood—since reverse phenotyping confirmed the upregulation of *IFNG* after stimulation, consistent with a functional Th1 definition[19]—these observations suggest that phenotypic and functional classifications of cell states may yield complementary conclusions.[20,21] This is particularly relevant given the uncertainty about how closely *ex vivo* stimulation conditions mimic antigen encounter *in vivo*. Unlike exploratory snapshot analyses performed after infection, a vaccination setting offers a unique opportunity for standardized, longitudinal investigation of antigen-reactive T cell phenotypes. The widespread SARS-CoV-2 vaccination campaign not only provided significant clinical benefits but also enabled rare, systematic studies of fundamental human T cell responses. Multiple studies have shown that repeated mRNA vaccination induces spike-reactive $CD4^+$ T cells with Th1/cTfh lineage characteristics and central/effector memory (TCM/TEM) differentiation states, mirroring responses seen in SARS-CoV-2 infection.[9,12,22–27] However, these studies were either limited to individual HLA class II-restricted epitopes or analyzed $CD4^+$ T cell phenotypes after antigenic restimulation *ex vivo*.

Here, we employed reverse phenotyping—complemented by DNA-barcoded pHLA class II dextramers for DPB1*04:01/S_{167} and T cell receptor (TCR) similarity metrics—to longitudinally characterize the phenotype of SARS-CoV-2 spike-reactive T cells both with and without *ex vivo* restimulation. Further validation using TCR-transgenic T cells revealed that, in the absence of restimulation, spike-reactive T cells during the memory phase predominantly exhibit a transcriptional profile consistent with a Th-neutral effector memory (TEM) state, lacking strong Th1 polarization. These Th-neutral signatures are otherwise obscured by the robust induction of Th1 programs observed in assays involving *ex vivo* restimulation. Overall, these data highlight the complementary value of different methods to identify and characterize antigen-reactive $CD4^+$ T cells.

RESULTS

Study design and analysis approach

Our previously published CoVa-Adapt cohort[28] consists of 29 healthy donors who received three SARS-CoV-2 mRNA (Comirnaty) vaccinations in a highly synchronized manner (Figure 1A and Table S1). A primary (P) vaccination was administered at day 0, followed by a secondary (S) vaccination at day 21 and a tertiary (T) vaccination at day 240. Blood samples were obtained 10 days after primary, secondary, and tertiary immunization (P10, S10, and T10), and additional memory time points were studied at S210, T108, and T189. 12–20 donors were subjected to a conventional assessment of spike antigen reactivity through an IFNγ ELISpot. In addition, two donors were analyzed by reverse phenotyping, exposing peripheral blood mononuclear cells (PBMCs) either to overlapping 15-mer peptide mixes of the spike antigen *ex vivo* or leaving them unstimulated. Donors A4 and A5 were selected for reverse phenotyping based on (1) high antigen reactivity after vaccination, ensuring sufficient numbers of antigen-reactive T cells for downstream analysis and (2) availability of sufficient cryopreserved material across multiple longitudinal time points. Subsequent flow cytometric sorting of non-naïve $CD4^+$ and $CD8^+$ T cells was followed by single-cell RNA sequencing (scRNAseq), including paired TCR sequencing (VDJseq) (Figure S1A and Table S2). For selected donors, we also performed epitope-specific scRNAseq analysis of $CD4^+$ T cells with pHLA class II dextramers for the DPB1*04:01/S_{167} spike epitope and CITEseq assessment of 130 surface proteins (Figure 1A and Table S3).

Identification and dynamics of reactive clonotypes

Visualization of scRNAseq data and concomitant Leiden clustering revealed one cluster (cluster 27), which was predominantly detected in the stimulated condition and mostly consisted of $CD4^+$ T cells (Figures S1B and S1C, and Table S4). This reactive cluster, in contrast to other clusters, showed marked upregulation of activation-related genes such as *IFNG* and of proliferation-associated genes despite the fact that *IFNG* or *TNF* were not among the top differentially expressed genes (DEG) identifying this cluster (Figures S1D–S1G). A principal component analysis (PCA) of

CoVa-Adapt donors were subjected to in-depth characterization using scRNAseq (reverse phenotyping and epitope-specific analyses) followed by TCR functional testing.

(B–G) scRNAseq data from the reverse phenotyping dataset. For reverse phenotyping, PBMCs were re-stimulated with 15-mer peptides covering the complete wild-type spike protein or left untreated. Sorted non-naïve $CD4^+$ and/or $CD8^+$ T cells were subjected to scRNAseq. Only $CD4^+$ T cells are shown (annotation described in the methods section). The full dataset is depicted in Figure S1. (B) UMAP of stimulated (blue) and unstimulated (orange) T cells (left) and Leiden clusters (right; cluster names in UMAP, cluster numbers on the right) (n = 101,939 cells in total). Cells located within the reactive cluster are displayed with increased point size. (C) Dot plots of log-normalized expression of representative genes per cluster. Selected genes of the reactive cluster are highlighted in gray. Numbers on the left indicate cluster numbers with reactive cluster 12 highlighted in bold. (D and E) *IFNG* expression (D) and proliferation score (E) in unstimulated (stimulated cells in gray) and stimulated (unstimulated cells in gray) $CD4^+$ T cells (left), and quantification in the stimulated condition of cells in the reactive cluster versus all other clusters (right). Cells located within the reactive cluster are displayed with increased point size. For *IFNG*, cells with log-normalized gene expression of 0 are shown in gray in UMAPs. Statistical testing by the Mann-Whitney U test. (F) UMAP visualization of cells classified as reactive (cells located in the reactive cluster or belonging to clones where at least one cell is in the reactive cluster) from donor A5 at individual time points after primary (P), secondary (S), and tertiary (T) vaccination in the stimulated condition. Color gradient indicates *IFNG* expression at the indicated time points. Non-reactive cells and cells from other donors are shown in gray. (G) Fraction of cells from donor A5 at each time point belonging to the reactive cluster.

(H and I) Identification of spike-reactive T cells after 20h of *in vitro* re-stimulation of PBMCs with 15-mer peptides covering the complete wild-type spike protein. Peptides were provided in two subpools, S1 (depicted in Figure 1H) and S2. Primary data (H) of donor A5 is shown. Quantification (I) of spot-forming units (SFU) for IFNγ ELISpot (combined frequencies of S1 and S2 subpools), data points represent individual donors (n = 12–19 per time point), solid lines indicate the mean. Samples without SFU above the negative control were set to not detected (n.d.). Donor A5 is highlighted in pink. Statistical testing by the Kruskal-Wallis test followed by Dunn's multiple comparisons test. Significant differences from the P10 time-point are indicated. $^{**}p < 0.01$, $^{****}p < 0.0001$, n.s. not significant.

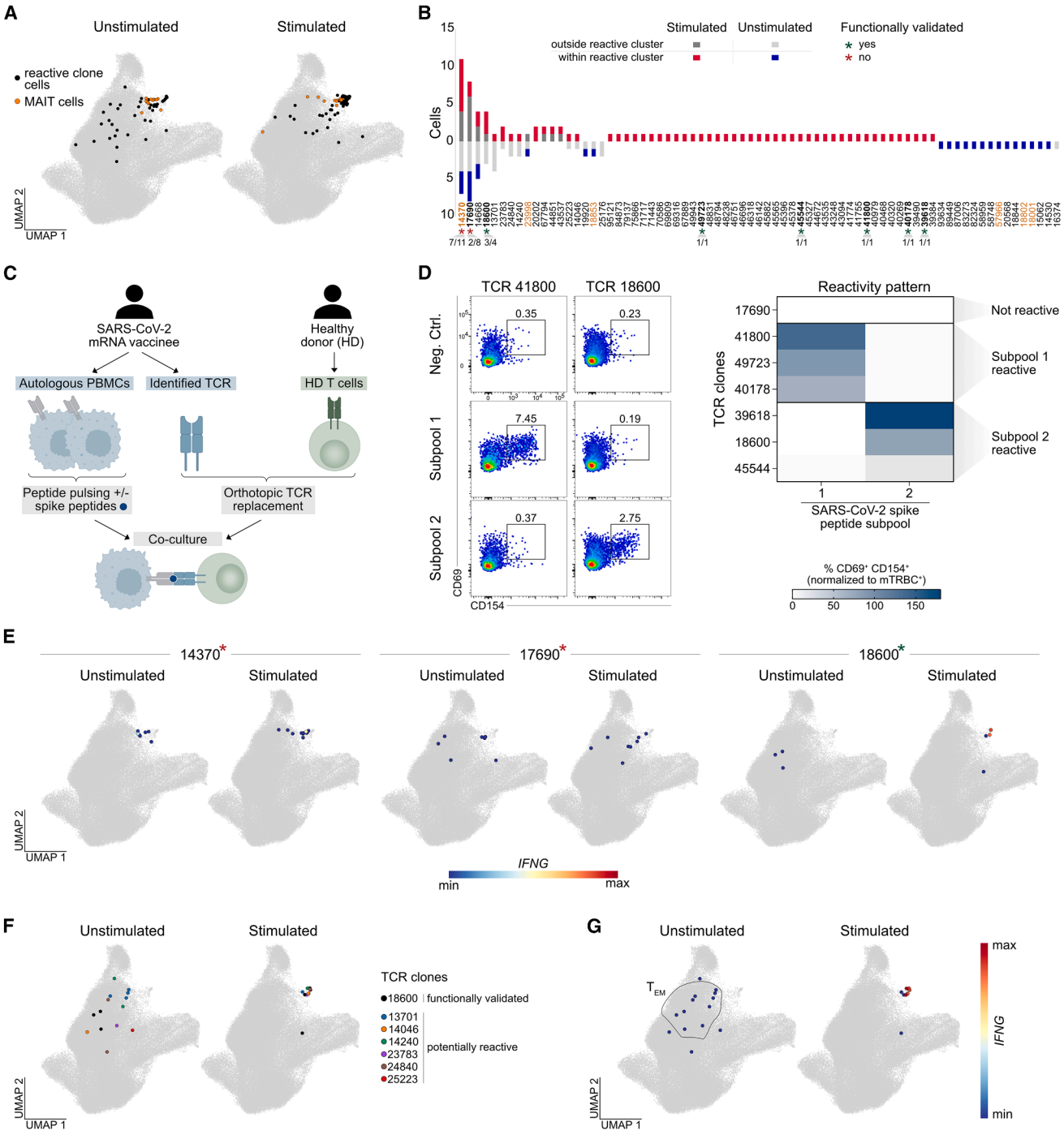

Figure 2. Functional validation of SARS-CoV-2 reactive T cell clones

(A) UMAP shows all cells classified as reactive (cells belonging to clones where at least one cell is in the reactive cluster) from donor A5 across all pooled time in the unstimulated (left; $n = 57$ cells) and stimulated (right; $n = 83$ cells) condition. Cells classified as MAIT cells (annotation described in the methods section) are depicted in orange. Non-reactive cells and cells from the other donor are shown in gray.

(B) Reactive clones of donor A5 are shown with the respective number of cells located within or outside the reactive cluster in the stimulated and unstimulated conditions. Clones identified as MAIT clones are highlighted in orange. Selected clones that were functionally validated and are shown in bold. For these clones, the fraction of cells recruited to the reactive cluster after re-stimulation is indicated at the bottom. Clones for which SARS-CoV-2 spike reactivity could be functionally validated are highlighted with a green asterisk, while non-reactive clones are marked by a red asterisk.

(C) Experimental setup for functional validation. T cells from healthy donors (HD T cells) were equipped with TCRs identified from donor A5 by CRISPR/Cas9-mediated orthotopic TCR replacement (OTR). Transgenic T cells were co-incubated with antigen-loaded PBMCs (serving as APCs) from donor A5. PBMCs were

(legend continued on next page)

pseudobulk reactive and unreactive T cell states from the stimulated or unstimulated condition showed that the T cell states from the two donors used for reverse phenotyping were highly similar in the unstimulated state (Figure S1H).

Peptide 15-mers likely more efficiently activate CD4$^+$ T cells compared to CD8$^+$ T cells.[29,30] We therefore focused subsequent analyses on CD4$^+$ T cells. New Leiden clustering of CD4$^+$ T cells yielded naïve-like (TN), TCM-like, TEM-like, and cytotoxic T cells, in addition to regulatory T cells and cycling cells (Figures 1B and 1C, and Table S5). TEM clusters 7, 11, and 2 displayed gradually higher *CCL5* expression, respectively, reflecting increasing differentiation states. The reactive cluster now mainly corresponded to cluster 12, showing elevated *IFNG* expression upon *ex vivo* restimulation (Figure 1D). Markers that are independent from distinct Th lineages, such as *CD40L* and a proliferation score, confirmed this assignment of the reactive cluster (Figure 1E and S2). We next performed a longitudinal assessment in the same donors (donor A5 shown in Figures 1F–1I; donor A4 shown in Figures S3A–S3D). This revealed that *IFNG* expression in reactive clones—defined as cells located in the reactive cluster itself or belonging to clones with sister cells in the reactive cluster—was pronounced at acute time points, particularly after secondary and tertiary immunization (Figure 1F and S3A). The dynamics of the magnitude of reactive cells thereby resembled IFNγ ELISpot analysis for the same donor (Figures 1G–1I and S3B–S3D), and also *IL2*, *TNF,* and *CD40L* showed similar kinetics (Figures S2 and S3A).

Validation of reactive clonotypes

We sought to validate that clonotypes recruited into the reactive cluster indeed represented SARS-CoV-2-reactive T cells. Intuitively, one would expect such clones to be recruited into the reactive cluster only in the stimulated condition, and to be among unreactive cells in the unstimulated condition. Investigating the phenotype and TCR sequence of cells in the reactive cluster in the unstimulated and stimulated conditions, we noted that several clonotypes in donor A5 (Figure 2A), but not in donor A4 (Figures S3E–S3G), corresponded to mucosal-associated invariant T (MAIT) cells. We quantified, for each clonotype, the number of cells present in the reactive cluster under stimulated or unstimulated conditions. We observed two particularly expanded clonotypes: the MAIT clone 14370 and the conventional clone 17690. Both clones were abundant in the reactive cluster, irrespective of the stimulation condition (Figure 2B). By contrast, other clonotypes, such as clone 18600, consisted exclusively of unreactive cells in the unstimulated condition but recruited most of their cells into the reactive cluster upon stimulation, thereby exhibiting the expected pattern of antigen-reactive T cells. We also identified many smaller clonotypes represented by single reactive cells under stimulation conditions (Figure 2B).

To functionally validate the antigen reactivity of these clonotypes, we performed CRISPR/Cas9-mediated orthotopic TCR replacement in unrelated primary human T cells from healthy donors. TCR-transgenic effector cells were co-cultured with spike antigen peptide-pulsed autologous PBMCs from SARS-CoV-2 mRNA-vaccinated donors to maintain HLA congruence (Figure 2C). This approach differentiated spike-reactive TCRs from non-reactive clonotypes. While clones such as 18600 or 41800 responded to sub-pools 1 or 2 of spike antigen, respectively, the expanded MAIT clone 14370 and clone 17690 both lacked reactivity (Figures 2D, S4, and S5). We confirmed the MAIT origin of TCR 14370 by a positive MR1 tetramer staining with the MAIT ligand 5-OP-RU next to prototypical TRAV1-2 expression (Figure S4C). The MAIT TCR 14370 neither reacted to spike antigen nor to the HLA class I-restricted SARS-CoV-2 epitope HLA-B*15:01/NQKLIANQF, which we tested because the recognition of this epitope is reported for the identical CDR3α and CDR3β chains in VDJdb[31] (Figure S4D). Overall, TCR re-expression in primary human T cells validated spike reactivity of non-MAIT clones that, in reverse phenotyping, showed specific recruitment to the reactive cluster upon stimulation.

Visualization of exemplary spike antigen-reactive or unreactive clonotypes in the UMAP space further demonstrated the specificity of this validation (Figures 2E and S6). Clones with unreactive TCRs—notably including MAIT clones such as 14370—showed a dispersed distribution across reactive and non-reactive clusters in both unstimulated and stimulated conditions, without specific upregulation of *IFNG* after stimulation. In contrast, validated clones such as 18600 displayed both selective recruitment into the reactive cluster and robust *IFNG* induction, but only in the stimulated condition. From here on, we excluded MAIT clones from our further analyses and concentrated on clones that are likely truly reactive, given a reactivity pattern resembling that of clone 18600, thereby also excluding clone 17690 (Figure 2F). Those clones were exclusively recruited

loaded with 1 μg/mL of 15-mer peptides covering the complete wildtype spike protein (provided in two separate subpools, S1 and S2) and reactivity was assessed by flow cytometry for activation marker expression.

(D) Primary data for two exemplary TCRs (left) after co-culture with SARS-CoV-2 spike peptide-loaded APCs (separately loaded with S1 and S2 peptide subpools). Data are pre-gated on living CD19$^-$ CD4$^+$ hTCR$^-$ lymphocytes. Quantification of CD69$^+$ CD154$^+$ double-positive CD4$^+$ T cells per clone (normalized to mTRBC$^+$ cells) after SARS-CoV-2 spike-specific stimulation with S1 or S2 subpools (right). Classification of clones as non-reactive, S1-reactive, or S2-reactive is indicated on the right. Only non-MAIT clones are shown. Functional characterization of MAIT clone 14370 is provided in Figure S4.

(E) *IFNG* expression in unstimulated or stimulated T cells for three representative clonotypes classified as reactive in donor A5. For each clonotype, cells belonging to that clonotype are shown in an individual paired panels (unstimulated condition on the left, stimulated condition on the right), while cells not belonging to that clonotype are shown in gray. Each clone is annotated with its functionally validated SARS-CoV-2 spike reactivity status (green asterisk = reactive; red asterisk = non-reactive). For the remaining functionally tested clones, see Figure S6A.

(F and G) Based on results from Figures 2A–2E, clones with cells located outside the reactive cluster in the unstimulated and within the reactive cluster in the stimulated condition were classified as potentially reactive clones. For donor A5, cells of these clones (n = 6) together with the functionally validated clone 18600 are depicted in the unstimulated (left) and stimulated condition (right) in the UMAP (F). Colors indicate cells belonging to the same clone. *IFNG* expression in unstimulated or stimulated T cells for these clones (G). Cells not belonging to these clonotypes are shown in gray. For visualization, log-transformed expression values > 3 were clipped.

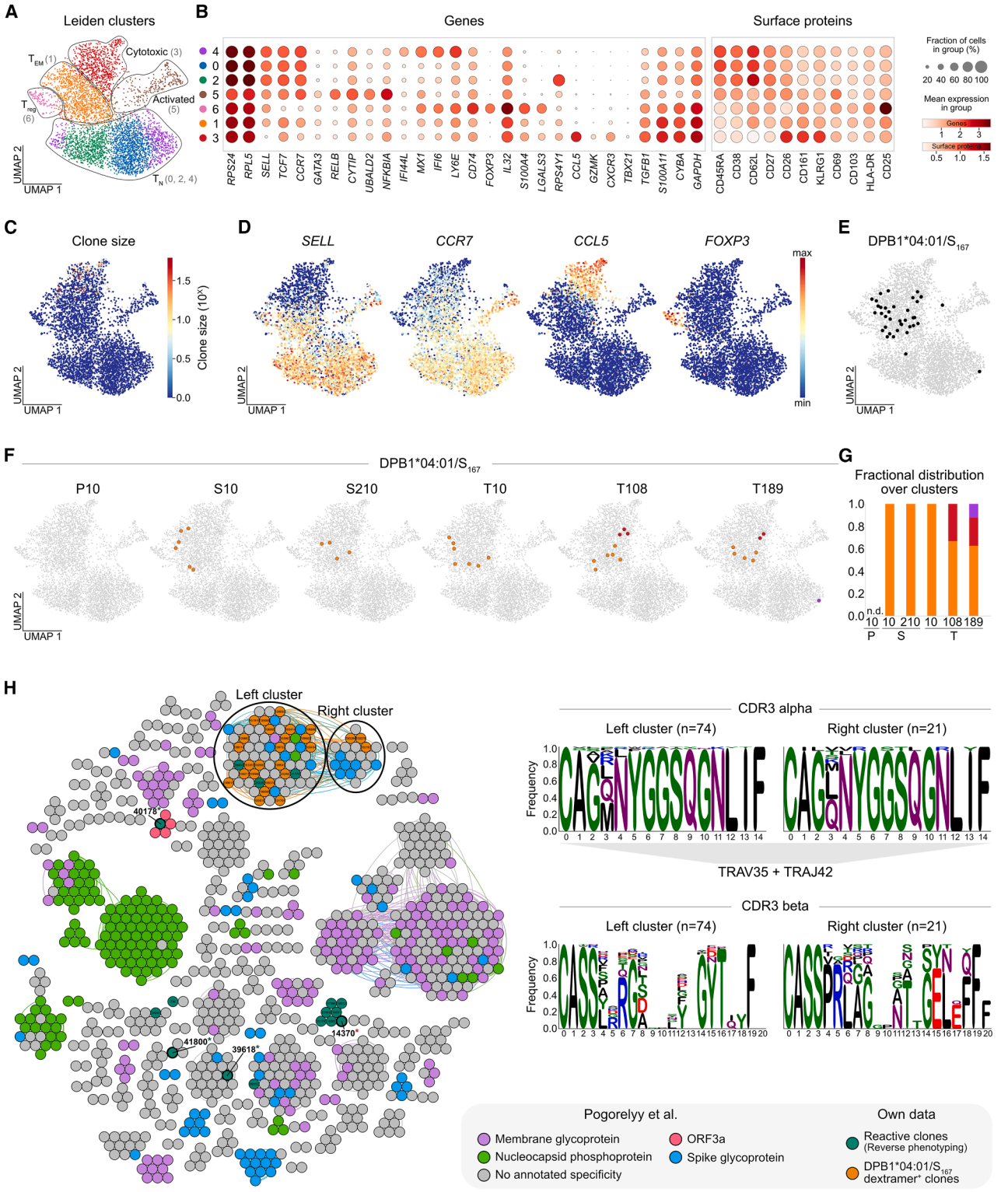

Figure 3. Identification of SARS-CoV-2-specific T cell responses by pHLA class II dextramers

(A) UMAP with Leiden clusters (cluster names in UMAP, cluster numbers on the right) of CD4+ T cells enriched for pHLA dextramer-binding (Figure S7A) (n = 4,882 cells).

(B) Dot plots show the log-normalized expression of representative genes and centered log-ratio (CLR) transformed expression of surface proteins per cluster. Numbers on the left indicate cluster numbers.

(legend continued on next page)

into the reactive cluster upon *ex vivo* stimulation, while without such stimulation, they were mostly found in the TEM clusters 7 and 11 (Figure 2G). Of note, the TEM clusters were characterized by low *TBX21* and *IFNG* expression (Figure 1C), highlighting the phenotypic changes antigen-reactive clones underwent upon antigenic stimulation *in vitro*.

Complementary validation by pHLA class II dextramers

Having established the reverse phenotyping approach for post-vaccination samples and having validated antigen-reactive clonotypes, we next sought to complement our analysis with an orthogonal strategy. To this end, we used pHLA class II dextramers for the S_{167} epitope (next to various pHLA class I dextramers for spike epitopes[28]) and performed scRNAseq and scTCRseq, including a CITEseq antibody cocktail for 130 surface proteins after flow cytometric sorting of $CD4^+$ and $CD8^+$ T cells (Figures S7A and S7B). Assignment of cells and clones as "dextramer-positive" depended on dextramer unique molecular identifier (UMI) counts as well as cellular and clonal purity thresholds for a given dextramer (see methods). S_{167}-binding clones could be unequivocally distinguished from clones binding to pHLA class I spike epitopes and were found in six out of seven tested donors, including a unique case of a hypervaccinated individual from Magdeburg (HIM) whose immune response to 217 SARS-CoV-2 vaccinations we previously characterized[32] (Figures S7C–S7H).

Clustering analysis based on transcriptomes identified regulatory T cells in cluster 6, activated T cells in cluster 5, naïve-like cells (TN) in clusters 4, 0, and 2, TEM-like cells in cluster 1, and cytotoxic $CD4^+$ cells in cluster 3 (Figures 3A and 3B, and Table S6). The cytotoxic cluster mostly contained expanded clonotypes and expressed *CCL5*, whereas the TEM-like cluster 1 partly maintained stemness markers such as *SELL* and *CCR7* (Figures 3C and 3D).

Dextramer-positive $CD4^+$ T cells binding the S_{167} epitope were markedly concentrated in the TEM-like cluster 1, which remained stable upon longitudinal assessment (Figures 3E–3G). Top DEG in this cluster 1 (Table S6) included *FTH1* (ferritin heavy chain 1), previously described in SARS-CoV-2 specific $CD4^+$ T cells with an intermediate differentiation degree[18]; *ZFP36* and *ZFP36L2*, which code for zing finger protein 36 family members that restrain full-blown T cell activation being RNA binding proteins[34]; and glycolysis/Th1 signature genes such as *GAPDH*, *AHNAK*, *ANXA1,* and *CYBA*.[35]

To integrate our reverse phenotyping approach with the dextramer data, we clustered antigen-reactive and dextramer-binding TCRs identified through both strategies based on sequence similarity (TCRdist[36]) together with previously published SARS-CoV-2-specific TCRs,[33] including TCRs reactive to the spike surface glycoprotein and the nucleocapsid phosphoprotein (Figure 3H). This revealed two large related clusters in which TCRs co-clustered that had been identified as spike-specific by our reverse phenotyping, by our dextramer analysis, and by others before.[33] The two presumably S_{167} reactive clusters exhibited similar, yet differing sequence motifs in their complementary determining regions of the TCRβ chain (CDR3β) and a striking convergence in CDR3α (Figure 3H) with a TRAV35/TRAJ42 bias (Figure S7I), which has been previously reported for TCR sequences recognizing this particular epitope.[8,27,37] This underlined the consistency of our approach and allowed us to distinguish TCRs identified through reverse phenotyping as likely specific for the S_{167} epitope from TCRs more likely directed to other regions of the spike protein.

Our integrated TCRdist analysis, powered by our validation experiments with TCR-transgenic T cells, also yielded other important observations. For example, it pointed to a presumably (false-positive) spike-reactive cluster entailing the non-validated clone 14370, highlighted alternative clusters recognizing the S_{167} epitope (including the validated clone 39618), and revealed a cluster designated as ORF3a-reactive entailing the validated spike-reactive clone 40178. Overall, this underlines the usefulness of integrating analyses with narrow epitope-specific and broad antigen-reactive resolution, and stresses the importance of reactivity validation through transgenic TCR re-expression.

Finally, we aimed to gain a comprehensive overview of phenotypic changes in reactive and unreactive clonotypes across stimulated and unstimulated conditions, and to compare these patterns to data obtained by complementary dextramer analyses. To do so, we analyzed exemplary genes associated with activation/effector cytokines, co-inhibition, differentiation, or lineage-defining transcription factors (Figure S8A). This confirmed that reactive clonotypes displayed higher *IFNG*, *TNF*, and *TNFRSF9* (gene of 4-1BB/CD137) expression compared to unreactive

(C) Visualization of clone sizes for all cells in the UMAP.

(D) Log-normalized expression of selected genes and scores.

(E) Visualization of SARS-CoV-2 spike epitope-specific T cells (DPB1*04:01/S_{167}: $n = 38$) across all HLA-matched donors (CoVa-Adapt donors and HIM; $n = 7$) and screened time points.

(F and G) UMAP visualization (F) and quantified fractional distribution (G) of DPB1*04:01/S_{167}-specific T cells of HLA-matched CoVa-Adapt donors excluding A7 due to breakthrough infection ($n = 5$) at individual time points after primary (P), secondary (S), and tertiary (T) vaccination. Colors represent the cluster location of epitope-specific cells at the respective time points. Cells without the indicated epitope-specificity are shown in gray. Time points with no detected epitope-specific cells are indicated as n.d.

(H) Similarity network of TCRs identified as reactive in the reverse phenotyping dataset (dark green) and of DPB1*04:01/S_{167} dextramer$^+$ TCR clones (orange) together with previously published SARS-CoV-2-specific TCRs[33] (left). Each vertex in the similarity network represents a unique paired αβTCR clonotype, and edges connect vertices with ≤120 TCRdist units. Only clusters containing at least two clonotypes are shown. Colors indicate SARS-CoV-2 epitope-specificity and dataset origin. Clonotypes without assigned specificity in the published dataset are shown in gray. Clone IDs from our own datasets are provided for each vertex, with functionally tested clones highlighted in bold. Clones for which SARS-CoV-2 spike reactivity could be functionally validated are highlighted with a green asterisk, while non-reactive clones are marked by a red asterisk. Two clusters containing our reactive and DPB1*04:01/S_{167}-specific clones, together with spike-annotated published clones, are highlighted (left and right clusters). Sequence motifs of CDR3α and CDR3β regions for the highlighted clusters are shown on the right. Amino acid positions are indicated at the bottom of each plot. For the CDR3α region, the dominantly used V- and J-gene segments are indicated below the motifs. For detailed V- and J-gene segment usage, see Figure S7I.

clonotypes already in the unstimulated condition, but the expression of these genes was markedly boosted by *ex vivo* stimulation. Interestingly, this boosting effect was more specific for *IFNG*, thereby being a poor *ex vivo* marker of reactive clones in the unstimulated state, while *TNF* and *TNFRSF9* segregated reactive from unreactive clones very well already without restimulation. Stimulation also expectedly accentuated the expression of co-inhibitory markers such as *PDCD1*, *LAG3*, and *CTLA4*, which were already expressed at higher levels in unstimulated reactive versus unreactive clonotypes. Reactive clonotypes further showed mild down-regulation of *CD27* and up-regulation of *ICOS* after stimulation. Of note, the Th1-defining transcription factor *TBX21*, encoding T-bet, was strongly up-regulated in reactive clonotypes upon stimulation, whereas in the absence of stimulation, *TBX21* expression levels were comparable to the Th2 (*GATA3*) or Tfh (*BCL6*) lineage-defining transcription factors.

Comparison with dextramer-positive cells further contextualized these findings (Figure S8B). While dextramer-positive T cells and reactive clonotypes from reverse phenotyping showed overall similar transcriptional profiles, some differences could be observed. For example, dextramer-positive clones exhibited low expression of *TNFRSF9* and *TNF* compared to unstimulated reactive clones, but high levels of *CCR7* and *CXCR4*. Compared to dextramer-negative cells, dextramer-positive cells showed more *TBX21* expression, but *GATA3* expression was even higher (Figure S8B), mirroring unstimulated reactive cells (Figure S8A).

DISCUSSION

Taken together, our data revealed transcriptional signatures in SARS-CoV-2 spike-reactive CD4$^+$ T cells following mRNA vaccination in the absence of *ex vivo* restimulation. Our findings confirmed an expected induction of activation markers upon *in-vitro* stimulation but placed this phenotypic plasticity into the context of the unperturbed *ex vivo* phenotypes.

The "Hawthorne effect" from behavioral psychology[38] describes how the act of measurement can itself alter the outcome. A similar concept exists in physics, where observation can influence the state of a system, as illustrated by Young's double-slit experiment[39] and Schrödinger's cat thought experiment.[40] Analogously, *in-vitro* restimulation of T cells acts as an observer effect: The process of restimulation alters the cells' phenotype, and the specific conditions of restimulation shape the resulting state. One might argue that a cell's functional state—what it does—is more relevant than its resting phenotype—what it looks like. In human immunology, however, it is often easier to describe the *ex vivo* phenotype compared to the *in vivo* function, although both readouts clearly possess complementary value. This discrepancy becomes important when the same T cell can display different activation profiles depending on the context.

For example, there is a long-standing discussion on how to define Th1 cells.[20,21,41] A functional definition classifies Th1 cells as those producing IFNγ upon stimulation. A transcriptional definition highlights the expression of the lineage-defining transcription factor T-bet (encoded by *TBX21*). If functional evaluation is not feasible, combinations of chemokine receptors are sometimes used as surrogates, in the case of Th1, for example, CXCR3.[41] While it would be correct to classify spike-reactive CD4$^+$ T cells as Th1 cells because they upregulate *IFNG* transcripts upon stimulation, in the resting state, they rather showed a "Th-neutral" phenotype, indicating plasticity depending on the stimulation conditions.

This has important implications for single-cell sequencing studies, which usually analyze cells in a resting state without restimulation. It is critical to recognize that such analyses capture a baseline phenotype and that transcription factor expression may not reflect what the same cells would look like after stimulation. For example, fungus-reactive CD4$^+$ T cells produce different cytokines than anti-viral CD4$^+$ T cells after stimulation.[19] The same caveat applies to *ex vivo* analyses using pHLA tetramers or dextramers, whether by flow cytometry or single-cell sequencing. The advantage of such approaches is that stimulation is not required, but the limitation is that the resulting phenotype will differ from that observed after *in vitro* or *in vivo* stimulation.

A strength of our study is the validation of TCRs after re-expression in primary human T cells. This revealed that some expanded clonotypes, including MAIT cells, were nonspecifically present in the reactive cluster under both stimulated and unstimulated conditions. Single-cell transcriptomes had already suggested that these were unlikely to represent true antigen-reactive CD4$^+$ T cells, since they did not show selective recruitment upon stimulation. TCR re-expression confirmed this suspicion by demonstrating a lack of spike reactivity. Without reverse phenotyping, such bystander clonotypes would likely have been misclassified as reactive. For example, had we simply stimulated PBMCs and sequenced all cells expressing activation markers or IFNγ, we would have included many of these expanded bystanders. Large clones may be particularly prone to this effect, as their size makes it more likely to sample cells in diverse activation or differentiation states.

In summary, our study demonstrates that reverse phenotyping combined with clonotypic tracking and functional TCR validation provides a powerful framework to dissect the biology of antigen-reactive T cells. By comparing stimulated and unstimulated states, we highlight the extent to which *in vitro* restimulation reshapes T cell phenotypes and how resting transcriptional states can nevertheless preserve a memory of past antigen encounter. These insights have direct implications for the interpretation of single-cell studies and for the classification of T cell subsets, reminding us that definitions based solely on either function or phenotype may be incomplete. More broadly, our work emphasizes the value of integrating orthogonal technologies—from unbiased transcriptomics to epitope-specific dextramers and functional TCR assays—to obtain a more accurate and nuanced understanding of human T cell immunity after vaccination.[42]

Limitations of the study

Several limitations of our study need to be acknowledged. In the unstimulated condition, we defined reactive clonotypes as those with cells in the reactive cluster, or as unstimulated clonotypes with sister cells in the reactive cluster in the stimulated condition. This definition introduces a potential bias toward clones detectable in the reactive cluster. Conceivably, there may be small clonotypes that never enter the reactive cluster in either condition. Such clonotypes would not be categorized as reactive by our approach. However, their relevance is likely limited, since they

are neither abundant nor show disproportionate recruitment upon stimulation. Another consideration is the number of donors available for reverse phenotyping. While our study applies this method for the first time in a standardized longitudinal setting, reverse phenotyping is highly cost-intensive. Large numbers of cells must be sequenced by scRNAseq across both stimulated and unstimulated conditions, without pre-enrichment for antigen reactivity. Although we pre-enriched for non-naïve T cells, thereby potentially excluding naïve-like or stem cell memory $CD4^+$ T cells, deep unbiased sequencing was still required to capture rare reactive clones with limited cell numbers. For this reason, we here studied only two donors by reverse phenotyping. However, we also do not view reverse phenotyping as a technique for routine donor characterization. Instead, we see it as a screening method for hypothesis generation to highlight the phenotypic biases introduced by restimulation and to reveal otherwise hidden states in the unstimulated condition. Subsequent targeted approaches, such as dextramer-based and functional assays, can then be used for more efficient analysis, including the assessment of molecular candidates on the protein level.

RESOURCE AVAILABILITY

Lead contact

Requests for further information and resources should be directed to the lead contact, Kilian Schober (kilian.schober@uk-erlangen.de).

Materials availability

This study did not generate new unique reagents. All data associated with this study are available in the article or the supplemental information.

Data and code availability

- Data: The single-cell sequencing data are publicly available at NCBI GEO under the accession numbers GSE310441 and GSE310442 for the reverse phenotyping dataset and GSE249998 for the dextramer dataset. The annotated data used for analysis is available on Zenodo under the accession doi:10.5281/zenodo.17091562.
- Code: The single-cell analysis code is available at https://github.com/SchubertLab/CovidVac_CD4.
- Other items: Any additional information required to reanalyze the data reported in this paper is available from the lead contact upon request

ACKNOWLEDGMENTS

This work is supported by grants from the German Federal Ministry of Research, Technology and Space (BMFTR, projects 01KI2013, 01KI2516, and 031L0290B), the Else Kröner-Fresenius-Stiftung (project 2020_EKEA.127) and the German Research Foundation (DFG) through the research training group RTG 2504 (project 401821119) to K.S.; and the BMFTR (project 031L0290A) to B.Sc. F.D. is supported by the Helmholtz Association under the joint research school "Munich School for Data Science - MUDS" and acknowledges financial support from the Joachim Herz Stiftung. Funding agencies had no influence on the study design or implementation.

We thank members from the Schober Laboratory for experimental support and critical discussion. We also thank Lucie Loyal (Berlin) and Petra Bacher (Kiel) for critical review of the manuscript. Furthermore, we also gratefully acknowledge the generous support of the Manfred Roth-Stiftung, Fürth, Germany, and thank the Core Unit Cell Sorting and Immunomonitoring Erlangen.

AUTHOR CONTRIBUTIONS

Conceptualization: K.S., data curation: K.K. and F.D., formal analysis: K.K. and F.D., funding acquisition: K.S. and B.Sc., investigation: K.K., F.D., C.S., and B.Sp., methodology: K.K., F.D., and K.S., project administration: K.S., resources: B.Sc. and K.S., software: F.D. and B.Sc., supervision: B.Sc. and K.S., validation: K.K. and F.D., visualization: K.K., F.D., and K.S., writing – original draft: K.K., F.D., and K.S., review and editing: all authors.

DECLARATION OF INTERESTS

The authors declare no competing interests.

DECLARATION OF GENERATIVE AI AND AI-ASSISTED TECHNOLOGIES IN THE WRITING PROCESS

During the preparation of this work, the authors used ChatGPT (GPT-5.3, OpenAI) in order to improve the readability and language of the manuscript. After using this tool, the authors reviewed and edited the content as needed and take full responsibility for the content of the published article.

STAR★METHODS

Detailed methods are provided in the online version of this paper and include the following:

SUPPLEMENTAL INFORMATION

Supplemental information can be found online at https://doi.org/10.1016/j.isci.2026.116175.

Received: December 5, 2025
Revised: March 2, 2026
Accepted: May 14, 2026

REFERENCES

1. Lee, Y., Tarke, A., and Grifoni, A. (2024). In-depth characterization of T cell responses with a combined Activation-Induced Marker (AIM) and Intracellular Cytokine Staining (ICS) assay. Oxf. Open Immunol. *5*, iqae014–iqae017. https://doi.org/10.1093/oxfimm/iqae014.
2. Szabo, P.A., Levitin, H.M., Miron, M., Snyder, M.E., Senda, T., Yuan, J., Cheng, Y.L., Bush, E.C., Dogra, P., Thapa, P., et al. (2019). Single-cell transcriptomics of human T cells reveals tissue and activation signatures in health and disease. Nat. Commun. *10*, 4706. https://doi.org/10.1038/s41467-019-12464-3.

3. Zheng, M.Z.M., Burmas, L., Tan, H.-X., Trieu, M.-C., Lee, H.J., Rawlinson, D., Haque, A.P., Kent, S.J., Wheatley, A.K., and Juno, J.A. (2025). Deconvoluting TCR-dependent and -independent activation is vital for reliable Ag-specific CD4+ T cell characterization by AIM assay. Sci. Adv. *11*, eadv3491. https://doi.org/10.1126/sciadv.adv3491.

4. Grifoni, A., Sidney, J., Vita, R., Peters, B., Crotty, S., Weiskopf, D., and Sette, A. (2022). SARS-CoV-2 human T cell epitopes: Adaptive immune response against COVID-19. Cell Host Microbe *30*, 1788. https://doi.org/10.1016/j.chom.2022.10.017.

5. Grifoni, A., Weiskopf, D., Ramirez, S.I., Mateus, J., Dan, J.M., Moderbacher, C.R., Rawlings, S.A., Sutherland, A., Premkumar, L., Jadi, R.S., et al. (2020). Targets of T Cell Responses to SARS-CoV-2 Coronavirus in Humans with COVID-19 Disease and Unexposed Individuals. Cell *181*, 1489–1501.e15. https://doi.org/10.1016/j.cell.2020.05.015.

6. Tarke, A., Sidney, J., Kidd, C.K., Dan, J.M., Ramirez, S.I., Yu, E.D., Mateus, J., da Silva Antunes, R., Moore, E., Rubiro, P., et al. (2021). Comprehensive analysis of T cell immunodominance and immunoprevalence of SARS-CoV-2 epitopes in COVID-19 cases. Cell Rep. Med. *2*, 100204. https://doi.org/10.1016/j.xcrm.2021.100204.

7. Loyal, L., Braun, J., Henze, L., Kruse, B., Dingeldey, M., Reimer, U., Kern, F., Schwarz, T., Mangold, M., Unger, C., et al. (2021). Cross-reactive CD4+ T cells enhance SARS-CoV-2 immune responses upon infection and vaccination. Science *374*, eabh1823. https://doi.org/10.1126/science.abh1823.

8. Mudd, P.A., Minervina, A.A., Pogorelyy, M.V., Turner, J.S., Kim, W., Kalaidina, E., Petersen, J., Schmitz, A.J., Lei, T., Haile, A., et al. (2022). SARS-CoV-2 mRNA vaccination elicits a robust and persistent T follicular helper cell response in humans. Cell *185*, 603–613.e15. https://doi.org/10.1016/j.cell.2021.12.026.

9. Wragg, K.M., Lee, W.S., Koutsakos, M., Tan, H.X., Amarasena, T., Reynaldi, A., Gare, G., Konstandopoulos, P., Field, K.R., Esterbauer, R., et al. (2022). Establishment and recall of SARS-CoV-2 spike epitope-specific CD4+ T cell memory. Nat. Immunol. *23*, 768–780. https://doi.org/10.1038/s41590-022-01175-5.

10. Koutsakos, M., Reynaldi, A., Lee, W.S., Nguyen, J., Amarasena, T., Taiaroa, G., Kinsella, P., Liew, K.C., Tran, T., Kent, H.E., et al. (2023). SARS-CoV-2 breakthrough infection induces rapid memory and de novo T cell responses. Immunity *56*, 879–892.e4. https://doi.org/10.1016/j.immuni.2023.02.017.

11. Lu, X., Hosono, Y., Nagae, M., Ishizuka, S., Ishikawa, E., Motooka, D., Ozaki, Y., Sax, N., Maeda, Y., Kato, Y., et al. (2021). Identification of conserved SARS-CoV-2 spike epitopes that expand public cTfh clonotypes in mild COVID-19 patients. J. Exp. Med. *218*, e20211327. https://doi.org/10.1084/jem.20211327.

12. Borcherding, N., Kim, W., Quinn, M., Han, F., Zhou, J.Q., Sturtz, A.J., Schmitz, A.J., Lei, T., Schattgen, S.A., Klebert, M.K., et al. (2024). CD4+ T cells exhibit distinct transcriptional phenotypes in the lymph nodes and blood following mRNA vaccination in humans. Nat. Immunol. *25*, 1731–1741. https://doi.org/10.1038/s41590-024-01888-9.

13. Fischer, D.S., Ansari, M., Wagner, K.I., Jarosch, S., Huang, Y., Mayr, C.H., Strunz, M., Lang, N.J., D'Ippolito, E., Hammel, M., et al. (2021). Single-cell RNA sequencing reveals ex vivo signatures of SARS-CoV-2-reactive T cells through 'reverse phenotyping. Nat. Commun. *12*, 4515. https://doi.org/10.1038/s41467-021-24730-4.

14. Sekine, T., Perez-Potti, A., Rivera-Ballesteros, O., Strålin, K., Gorin, J.-B., Olsson, A., Llewellyn-Lacey, S., Kamal, H., Bogdanovic, G., Muschiol, S., et al. (2020). Robust T Cell Immunity in Convalescent Individuals with Asymptomatic or Mild COVID-19. Cell *183*, 158–168.e14. https://doi.org/10.1016/j.cell.2020.08.017.

15. Weiskopf, D., Schmitz, K.S., Raadsen, M.P., Grifoni, A., Okba, N.M.A., Endeman, H., van den Akker, J.P.C., Molenkamp, R., Koopmans, M.P.G., van Gorp, E.C.M., et al. (2020). Phenotype and kinetics of SARS-CoV-2-specific T cells in COVID-19 patients with acute respiratory distress syndrome. Sci. Immunol. *5*, eabd2071. https://doi.org/10.1126/sciimmunol.abd2071.

16. Rydyznski Moderbacher, C., Ramirez, S.I., Dan, J.M., Grifoni, A., Hastie, K.M., Weiskopf, D., Belanger, S., Abbott, R.K., Kim, C., Choi, J., et al. (2020). Antigen-Specific Adaptive Immunity to SARS-CoV-2 in Acute COVID-19 and Associations with Age and Disease Severity. Cell *183*, 996–1012.e19. https://doi.org/10.1016/j.cell.2020.09.038.

17. Meckiff, B.J., Ramírez-Suástegui, C., Fajardo, V., Chee, S.J., Kusnadi, A., Simon, H., Eschweiler, S., Grifoni, A., Pelosi, E., Weiskopf, D., et al. (2020). Imbalance of Regulatory and Cytotoxic SARS-CoV-2-Reactive CD4+ T Cells in COVID-19. Cell *183*, 1340–1353.e16. https://doi.org/10.1016/j.cell.2020.10.001.

18. Bacher, P., Rosati, E., Esser, D., Martini, G.R., Saggau, C., Schiminsky, E., Dargvainiene, J., Schröder, I., Wieters, I., Khodamoradi, Y., et al. (2020). Low-Avidity CD4+ T Cell Responses to SARS-CoV-2 in Unexposed Individuals and Humans with Severe COVID-19. Immunity *53*, 1258–1271.e5. https://doi.org/10.1016/j.immuni.2020.11.016.

19. Bacher, P., Schink, C., Teutschbein, J., Kniemeyer, O., Assenmacher, M., Brakhage, A.A., and Scheffold, A. (2013). Antigen-Reactive T Cell Enrichment for Direct, High-Resolution Analysis of the Human Naive and Memory Th Cell Repertoire. J. Immunol. *190*, 3967–3976. https://doi.org/10.4049/jimmunol.1202221.

20. Mosmann, T.R., Cherwinski, H., Bond, M.W., Giedlin, M.A., and Coffman, R.L. (1986). Two types of murine helper T cell clone. I. Definition according to profiles of lymphokine activities and secreted proteins. J. Immunol. *136*, 2348–2357.

21. Morimoto, C., Letvin, N.L., Distaso, J.A., Aldrich, W.R., and Schlossman, S.F. (1985). The isolation and characterization of the human suppressor inducer T cell subset. J. Immunol. *134*, 1508–1515.

22. Sette, A., Sidney, J., and Crotty, S. (2023). T Cell Responses to SARS-CoV-2. Annu. Rev. Immunol. *41*, 343–373. https://doi.org/10.1146/annurev-immunol-101721-061120.

23. Chen, Z., and John Wherry, E. (2020). T cell responses in patients with COVID-19. Nat. Rev. Immunol. *20*, 529–536. https://doi.org/10.1038/s41577-020-0402-6.

24. Kedzierska, K., and Thomas, P.G. (2022). Count on us: T cells in SARS-CoV-2 infection and vaccination. Cell Rep. Med. *3*, 100562. https://doi.org/10.1016/j.xcrm.2022.100562.

25. Painter, M.M., Mathew, D., Goel, R.R., Apostolidis, S.A., Pattekar, A., Kuthuru, O., Baxter, A.E., Herati, R.S., Oldridge, D.A., Gouma, S., et al. (2021). Rapid induction of antigen-specific CD4+ T cells is associated with coordinated humoral and cellular immunity to SARS-CoV-2 mRNA vaccination. Immunity *54*, 2133–2142.e3. https://doi.org/10.1016/j.immuni.2021.08.001.

26. Goel, R.R., Painter, M.M., Apostolidis, S.A., Mathew, D., Meng, W., Rosenfeld, A.M., Lundgreen, K.A., Reynaldi, A., Khoury, D.S., Pattekar, A., et al. (2021). mRNA vaccines induce durable immune memory to SARS-CoV-2 and variants of concern. Science *374*, abm0829. https://doi.org/10.1126/science.abm0829.

27. Saggau, C., Martini, G.R., Rosati, E., Meise, S., Messner, B., Kamps, A.-K., Bekel, N., Gigla, J., Rose, R., Voß, M., et al. (2022). The pre-exposure SARS-CoV-2-specific T cell repertoire determines the quality of the immune response to vaccination. Immunity *55*, 1924–1939.e5. https://doi.org/10.1016/j.immuni.2022.08.003.

28. Kocher, K., Drost, F., Tesfaye, A.M., Moosmann, C., Schülein, C., Grotz, M., D'Ippolito, E., Graw, F., Spriewald, B., Busch, D.H., et al. (2025). Vaccination-induced T cell responses maintain polyclonality with high antigen receptor avidity. Sci. Immunol. *10*, eadu6730. https://doi.org/10.1126/sciimmunol.adu6730.

29. Cossarizza, A., Chang, H.-D., Radbruch, A., Andrä, I., Andrä, I., Annunziato, F., Bacher, P., Barnaba, V., Battistini, L., Bauer, W.M., et al. (2017). Guidelines for the use of flow cytometry and cell sorting in immunological studies. Eur. J. Immunol. *47*, 1584–1797. https://doi.org/10.1002/eji.201646632.

30. Lehmann, P.V., Suwansaard, M., Zhang, T., Roen, D.R., Kirchenbaum, G.A., Karulin, A.Y., Lehmann, A., and Reche, P.A. (2019). Comprehensive

Evaluation of the Expressed CD8+ T Cell Epitope Space Using High-Throughput Epitope Mapping. Front. Immunol. *10*, 655. https://doi.org/10.3389/fimmu.2019.00655.

31. Goncharov, M., Bagaev, D., Shcherbinin, D., Zvyagin, I., Bolotin, D., Thomas, P.G., Minervina, A.A., Pogorelyy, M.V., Ladell, K., McLaren, J.E., et al. (2022). VDJdb in the pandemic era: a compendium of T cell receptors specific for SARS-CoV-2. Nat. Methods *19*, 1017–1019. https://doi.org/10.1038/s41592-022-01578-0.

32. Kocher, K., Moosmann, C., Drost, F., Schülein, C., Irrgang, P., Steininger, P., Zhong, J., Träger, J., Spriewald, B., Bock, C., et al. (2024). Adaptive immune responses are larger and functionally preserved in a hypervaccinated individual. Lancet Infect. Dis. *24*, e272–e274. https://doi.org/10.1016/S1473-3099(24)00134-8.

33. Pogorelyy, M.V., Rosati, E., Minervina, A.A., Mettelman, R.C., Scheffold, A., Franke, A., Bacher, P., and Thomas, P.G. (2022). Resolving SARS-CoV-2 CD4+ T cell specificity via reverse epitope discovery. Cell Rep. Med. *3*, 100697. https://doi.org/10.1016/j.xcrm.2022.100697.

34. Cook, M.E., Bradstreet, T.R., Webber, A.M., Kim, J., Santeford, A., Harris, K.M., Murphy, M.K., Tran, J., Abdalla, N.M., Schwarzkopf, E.A., et al. (2022). The ZFP36 family of RNA binding proteins regulates homeostatic and autoreactive T cell responses. Sci. Immunol. *7*, eabo0981. https://doi.org/10.1126/sciimmunol.abo0981.

35. Ciucci, T., Vacchio, M.S., Gao, Y., Tomassoni Ardori, F., Candia, J., Mehta, M., Zhao, Y., Tran, B., Pepper, M., Tessarollo, L., et al. (2019). The Emergence and Functional Fitness of Memory CD4+ T Cells Require the Transcription Factor Thpok. Immunity *50*, 91–105.e4. https://doi.org/10.1016/j.immuni.2018.12.019.

36. Mayer-Blackwell, K., Schattgen, S., Cohen-Lavi, L., Crawford, J.C., Souquette, A., Gaevert, J.A., Hertz, T., Thomas, P.G., Bradley, P., and Fiore-Gartland, A. (2021). Tcr meta-clonotypes for biomarker discovery with tcrdist3 enabled identification of public, hla-restricted clusters of sars-cov-2 tcrs. eLife *10*, e68605. https://doi.org/10.7554/eLife.68605.

37. Rowntree, L.C., Nguyen, T.H.O., Kedzierski, L., Neeland, M.R., Petersen, J., Crawford, J.C., Allen, L.F., Clemens, E.B., Chua, B., McQuilten, H.A., et al. (2022). SARS-CoV-2-specific T cell memory with common TCRαβ motifs is established in unvaccinated children who seroconvert after infection. Immunity *55*, 1299–1315.e4. https://doi.org/10.1016/j.immuni.2022.06.003.

38. Roethlisberger, F.J., and Dickson, W.J. (1939). Management and the Worker (Psychology press).

39. Young, T. (1804). I. The Bakerian Lecture. Experiments and calculations relative to physical optics. Philos. Trans. R. Soc. London, A *94*, 1–16. https://doi.org/10.1098/rstl.1804.0001.

40. Schrödinger, E. (1935). Die gegenwärtige Situation in der Quantenmechanik. Naturwissenschaften *23*, 807–812. https://doi.org/10.1007/BF01491891.

41. Sallusto, F. (2016). Heterogeneity of Human CD4+ T Cells Against Microbes. Annu. Rev. Immunol. *34*, 317–334. https://doi.org/10.1146/annurev-immunol-032414-112056.

42. Seder, R.A., Darrah, P.A., and Roederer, M. (2008). T-cell quality in memory and protection: Implications for vaccine design. Nat. Rev. Immunol. *8*, 247–258. https://doi.org/10.1038/nri2274.

43. Wolf, F.A., Angerer, P., and Theis, F.J. (2018). SCANPY: large-scale single-cell gene expression data analysis. Genome Biol. *19*, 15. https://doi.org/10.1186/s13059-017-1382-0.

44. Sturm, G., Szabo, T., Fotakis, G., Haider, M., Rieder, D., Trajanoski, Z., and Finotello, F. (2020). Scirpy: a Scanpy extension for analyzing single-cell T-cell receptor-sequencing data. Bioinformatics *36*, 4817–4818. https://doi.org/10.1093/bioinformatics/btaa611.

45. Bernstein, N.J., Fong, N.L., Lam, I., Roy, M.A., Hendrickson, D.G., and Kelley, D.R. (2020). Solo: Doublet Identification in Single-Cell RNA-Seq via Semi-Supervised Deep Learning. Cell Syst. *11*, 95–101.e5. https://doi.org/10.1016/j.cels.2020.05.010.

46. Edgar, R.C. (2004). MUSCLE: A multiple sequence alignment method with reduced time and space complexity. BMC Bioinf. *5*, 113. https://doi.org/10.1186/1471-2105-5-113.

47. Tareen, A., and Kinney, J.B. (2020). Logomaker: Beautiful sequence logos in Python. Bioinformatics *36*, 2272–2274. https://doi.org/10.1093/bioinformatics/btz921.

48. Irrgang, P., Gerling, J., Kocher, K., Lapuente, D., Steininger, P., Habenicht, K., Wytopil, M., Beileke, S., Schäfer, S., Zhong, J., et al. (2023). Class switch toward noninflammatory, spike-specific IgG4 antibodies after repeated SARS-CoV-2 mRNA vaccination. Sci. Immunol. *8*, eade2798. https://doi.org/10.1126/sciimmunol.ade2798.

49. Heumos, L., Schaar, A.C., Lance, C., Litinetskaya, A., Drost, F., Zappia, L., Lücken, M.D., Strobl, D.C., Henao, J., Curion, F., et al. (2023). Best practices for single-cell analysis across modalities. Nat. Rev. Genet. *24*, 550–572. https://doi.org/10.1038/s41576-023-00586-w.

50. Seumois, G., Ramírez-Suástegui, C., Schmiedel, B.J., Liang, S., Peters, B., Sette, A., and Vijayanand, P. (2020). Single-cell transcriptomic analysis of allergen-specific T cells in allergy and asthma. Sci. Immunol. *5*, eaba6087. https://doi.org/10.1126/sciimmunol.aba6087.

51. Traag, V.A., Waltman, L., and van Eck, N.J. (2019). From Louvain to Leiden: guaranteeing well-connected communities. Sci. Rep. *9*, 5233. https://doi.org/10.1038/s41598-019-41695-z.

52. McInnes, L., Healy, J., Saul, N., and Großberger, L. (2018). UMAP: Uniform Manifold Approximation and Projection. J. Open Source Softw. *3*, 861. https://doi.org/10.21105/joss.00861.

53. Bastian, M., Heymann, S., and Jacomy, M. (2009). Gephi: An Open Source Software for Exploring and Manipulating Networks. Proc. Int. AAAI Conf. Web Soc. Media *3*, 361–362. https://doi.org/10.1609/icwsm.v3i1.13937.

54. Schober, K., Müller, T.R., Gökmen, F., Grassmann, S., Effenberger, M., Poltorak, M., Stemberger, C., Schumann, K., Roth, T.L., Marson, A., and Busch, D.H. (2019). Orthotopic replacement of T-cell receptor α- and β-chains with preservation of near-physiological T-cell function. Nat. Biomed. Eng. *3*, 974–984. https://doi.org/10.1038/s41551-019-0409-0.

55. Moosmann, C., Müller, T.R., Busch, D.H., and Schober, K. (2022). Orthotopic T-cell receptor replacement in primary human T cells using CRISPR-Cas9-mediated homology-directed repair. STAR Protoc. *3*, 101031. https://doi.org/10.1016/j.xpro.2021.101031.

56. Cohen, C.J., Li, Y.F., El-Gamil, M., Robbins, P.F., Rosenberg, S.A., and Morgan, R.A. (2007). Enhanced antitumor activity of T cells engineered to express T-cell receptors with a second disulfide bond. Cancer Res. *67*, 3898–3903. https://doi.org/10.1158/0008-5472.CAN-06-3986.

57. Ren, J., Liu, X., Fang, C., Jiang, S., June, C.H., and Zhao, Y. (2017). Multiplex Genome Editing to Generate Universal CAR T Cells Resistant to PD1 Inhibition. Clin. Cancer Res. *23*, 2255–2266. https://doi.org/10.1158/1078-0432.CCR-16-1300.

58. Kath, J., Du, W., Pruene, A., Braun, T., Thommandru, B., Turk, R., Sturgeon, M.L., Kurgan, G.L., Amini, L., Stein, M., et al. (2022). Pharmacological interventions enhance virus-free generation of TRAC-replaced CAR T cells. Mol. Ther. Methods Clin. Dev. *25*, 311–330. https://doi.org/10.1016/j.omtm.2022.03.018.

59. Nguyen, D.N., Roth, T.L., Li, P.J., Chen, P.A., Apathy, R., Mamedov, M.R., Vo, L.T., Tobin, V.R., Goodman, D., Shifrut, E., et al. (2020). Polymer-stabilized Cas9 nanoparticles and modified repair templates increase genome editing efficiency. Nat. Biotechnol. *38*, 44–49. https://doi.org/10.1038/s41587-019-0325-6.

60. Shy, B.R., Vykunta, V.S., Ha, A., Talbot, A., Roth, T.L., Nguyen, D.N., Pfeifer, W.G., Chen, Y.Y., Blaeschke, F., Shifrut, E., et al. (2023). High-yield genome engineering in primary cells using a hybrid ssDNA repair template and small-molecule cocktails. Nat. Biotechnol. *41*, 521–531. https://doi.org/10.1038/s41587-022-01418-8.

STAR★METHODS

KEY RESOURCES TABLE

REAGENT or RESOURCE	SOURCE	IDENTIFIER
Antibodies		
BD Horizon™ BUV395 Mouse Anti-Human CD4	BD Biosciences	Cat#564724; RRID:AB_2738917
BD Horizon™ PE-CF594 Mouse Anti-Human CD19	BD Biosciences	Cat#562294; RRID:AB_11154408
BD Pharmingen™ PerCP-Cy™5.5 Mouse Anti-Human CD69	BD Biosciences	Cat#560738; RRID:AB_1727510
BD FastImmune™ FITC Mouse Anti-Human IFN-γ	BD Biosciences	Cat#340449; RRID:AB_400425
BD FastImmune™ APC Mouse Anti-Human IL-2	BD Biosciences	Cat#341116; RRID:AB_400574
Brilliant Violet 510™ anti-human CD4 Antibody	BioLegend	Cat#300545; RRID:AB_2563313
APC anti-human CD8a Antibody	BioLegend	Cat#301049; RRID:AB_2562054
FITC anti-human TCR α/β Antibody	BioLegend	Cat#306706; RRID:AB_314644
APC/Fire™ 750 anti-mouse TCR β chain Antibody	BioLegend	Cat#109246; RRID:AB_2629697
PerCP/Cyanine5.5 anti-human CD45RA Antibody	BioLegend	Cat#304121; RRID:AB_893358
Pacific Blue™ anti-human CD62L Antibody	BioLegend	Cat#304825; RRID:AB_2301675
PerCP/Cyanine5.5 anti-human CD154 (CD40L) Antibody	BioLegend	Cat#310833; RRID:AB_2563114
PE/Cyanine7 anti-human CD137 (4-1BB) Antibody	BioLegend	Cat#309817; RRID:AB_2287731
Brilliant Violet 711™ anti-human TCR Vα7.2 Antibody	BioLegend	Cat#351731; RRID:AB_2629679
CD4 Monoclonal Antibody (RPA-T4), PE, eBioscience™	Thermo Fisher Scientific	Cat#12-0049-42; RRID:AB_1582249
CD8a Monoclonal Antibody (OKT8 (OKT-8)), eFluor™ 450, eBioscience™	Thermo Fisher Scientific	Cat#48-0086-42; RRID:AB_1907412
CD56 (NCAM) Monoclonal Antibody (TULY56), FITC, eBioscience™	Thermo Fisher Scientific	Cat#11-0566-42; RRID:AB_2572459
CD45 Monoclonal Antibody (HI30), PerCP-Cyanine5.5, eBioscience™	Thermo Fisher Scientific	Cat#45-0459-42; RRID:AB_10717530
CD45 Monoclonal Antibody (2D1), PE-Cyanine7, eBioscience™	Thermo Fisher Scientific	Cat#25-9459-42; RRID:AB_2573544
Monoclonal Mouse Anti-Human CD45, Leukocyte Common Antigen, PacificBlue	Agilent Technologies	Cat#PB98601-8
CD154 Antibody, anti-human, APC	Miltenyi	Cat#130-113-603; RRID:AB_2726191
Anti-human IFN-γ mAb (1-D1K), unconjugated	Mabtech	Cat#3420-3-1000; RRID:AB_907282
Anti-human IFN-γ mAb (7-B6-1), biotin	Mabtech	Cat#3420-6-250; RRID:AB_907273
TotalSeq™-C0251 anti-human Hashtag 1 Antibody	BioLegend	Cat#394661; RRID:AB_2801031
TotalSeq™-C0252 anti-human Hashtag 2 Antibody	BioLegend	Cat#394663; RRID:AB_2801032
TotalSeq™-C0253 anti-human Hashtag 3 Antibody	BioLegend	Cat#394665; RRID:AB_2801033
TotalSeq™-C0254 anti-human Hashtag 4 Antibody	BioLegend	Cat#394667; RRID:AB_2801034
TotalSeq™-C0255 anti-human Hashtag 5 Antibody	BioLegend	Cat#394669; RRID:AB_2801035
TotalSeq™-C0256 anti-human Hashtag 6 Antibody	BioLegend	Cat#394671; RRID:AB_2820042
TotalSeq™-C0257 anti-human Hashtag 7 Antibody	BioLegend	Cat#394673; RRID:AB_2820043
TotalSeq™-C0258 anti-human Hashtag 8 Antibody	BioLegend	Cat#394675; RRID:AB_2820044
TotalSeq™-C0063 anti-human CD45RA Antibody	BioLegend	Cat#304163; RRID:AB_2800764
TotalSeq™-C0148 anti-human CD197 (CCR7) Antibody	BioLegend	Cat#353251; RRID:AB_2800943
TotalSeq™-C0140 anti-human CD183 (CXCR3) Antibody	BioLegend	Cat#353747; RRID:AB_2800949
Purified anti-human CD3 Antibody	BioLegend	Cat#317302; RRID:AB_571927

(*Continued on next page*)

Continued

REAGENT or RESOURCE	SOURCE	IDENTIFIER
Purified anti-human CD28 Antibody	BioLegend	Cat#302902; RRID:AB_314304
Biological samples		
Healthy donor blood samples	Transfusion Medicine, University Hospital Erlangen, Germany	N/A
Chemicals, peptides, and recombinant proteins		
RPMI 1640 Medium	Thermo Fisher Scientific	Cat#21875091
Heat-Inactivated Fetal Bovine Serum (South America)	anprotec	Cat#AC-SM-0027
β-Mercaptoethanol (50 mM)	Thermo Fisher Scientific	Cat#31350010
Gentamicin (50 mg/mL)	Thermo Fisher Scientific	Cat#15750060
HEPES	Carl Roth	Cat#HN77.3; CAS: 7365-45-9
L-Glutamine	Sigma-Aldrich	Cat#G8540; CAS: 56-85-9
Penicillin-Streptomycin (10,000 U/mL)	Thermo Fisher Scientific	Cat#15140122
Ethidium-Monoazide-Bromide	Thermo Fisher Scientific	Cat# E1374
Propidium Iodide	Thermo Fisher Scientific	Cat#P1304MP; CAS: 25535-16-4
Phorbol Myristate Acetate	Sigma-Aldrich	Cat# P1585-1 mg
Ionomycin	Sigma-Aldrich	Cat# I9657-1 MG
Tween 20	Sigma-Aldrich	Cat# P9416-50 mL
AEC substrate solution	Sigma-Aldrich	Cat#152224-10 mL
PepMix™ SARS-CoV-2 spike glycoprotein peptide pool	JPT	Cat#PM-WCPV-S-2
PepMix™ SARS-CoV-2 nucleoprotein peptide pool	JPT	Cat# PM-WCPV-NCAP-2
NQKLIANQF peptide	peptides&elephants	N/A
Recombinant Human IL-2	PeproTech	Cat#200-02; Accession Number: P60568
Recombinant Human IL-7	PeproTech	Cat#200-07; Accession Number: P13232
Recombinant Human IL-15	PeproTech	Cat#200-15; Accession Number: P40933
Poly-L-glutamic acid sodium salt, mol wt 15,000–50,000 (PGA)	Sigma-Aldrich	Cat#P4761-100 mg; CAS: 26247-79-0
Alt-R® S.p. Cas9 Nuclease V3	Integrated DNA Technologies	Cat#1081059
RU.521 (small-molecule inhibitor of cyclic GMP-AMP synthase (cGAS)	InvivoGen	Cat#inh-ru521
HDAC class I/II Inhibitor Trichostatin A	AbMole	Cat#M1753
DNA-dependent protein kinase (DNA-PK) inhibitor M3814	chemietek	Cat#CT-M3814
Critical commercial assays		
ZombieNIR Fixable Viability Kit	BioLegend	Cat#423106
BD Cytofix/Cytoperm Kit	BD Biosciences	Cat#554714
VECTASTAIN® Elite ABC-HRP Kit	Vector Laboratories	Cat#VEC-PK-6100
Chromium Next GEM Single Cell 5′ Kit v2	10× Genomics	Cat#PN-1000263
Chromium Single Cell Human TCR Amplification Kit	10× Genomics	Cat#PN-1000252
Chromium Next GEM Chip K Single Cell Kit	10× Genomics	Cat#PN-1000286
Dual Index Kit TN Set A	10× Genomics	Cat#PN-1000250
Dual Index Kit TT Set A	10× Genomics	Cat#PN-1000215
Library Construction Kit	10× Genomics	Cat#PN-1000190
5′ Feature Barcode Kit	10× Genomics	Cat#PN-1000541
TotalSeq-C Human Universal Cocktail, V1.0	BioLegend	Cat#399905
P3 Primary Cell 96-well Nucleofector™ Kit (960 RCT)	Lonza	Cat#V4SP-3960
Deposited data		
Processed dataset	In house	https://doi.org/10.5281/zenodo.17091561
Raw single-cell sequencing data – Dextramer dataset	In house	GSE249998

(*Continued on next page*)

Continued

REAGENT or RESOURCE	SOURCE	IDENTIFIER
Raw single-cell sequencing data – Reverse Phenotyping dataset – Part 1	In house	GSE310441
Raw single-cell sequencing data – Reverse Phenotyping dataset – Part 2	In house	GSE310442
Oligonucleotides		
hTRAC HDR genomic forward primer targeting LHA (5′-TCTCTCTCTCAGCTGG TACACGGCTGCCTTTACTCTGCCAGAG-3′)	Eurofins; Müller et al. (2021)	N/A
hTRAC HDR genomic reverse primer targeting RHA (5′-CATCATTGACCAGAGCTCTG-3′)	Eurofins; Müller et al. (2021)	N/A
Alt-R® CRISPR-Cas9 tracrRNA	Integrated DNA Technologies	Cat#1072534
hTRAC crRNA (5′-AGAGTCTCTCAGCTGGTACA-3′)	Integrated DNA Technologies; Ren et al. (2017)	N/A
hTRBC crRNA (5′-GGAGAATGACGAGTGGACCC-3′)	Integrated DNA Technologies; Schober et al. (2019)	N/A
Alt-R® Cas9 Electroporation Enhancer	Integrated DNA Technologies	Cat#10007805
Recombinant DNA		
HDR DNA template sequence	Twist Bioscience	N/A
Software and algorithms		
FlowJo (version 10.7.2)	BD Biosciences	https://www.flowjo.com/
GraphPad Prism 10 software	GraphPad software	https://www.graphpad.com/
Affinity Designer	Serif (Europe) Ltd	https://www.affinity.studio/en
Cellranger	10× Genomics	V.6.0.2
Scanpy	Wolf et al.[43]	Pip V.1.8.2
Scirpy	Sturm et al.[44]	Pip V.0.10.1
HashSolo	Bernstein et al.[45]	Pip V.1.8.2
TCRdist3	Mayer-Blackwell et al.[36]	Pip V.0.2.2
Gephi	Gephi Consortium	V.0.9.7
MUSCLE	Edgar et al.[46]	https://ebi.ac.uk/jdispatcher/msa/muscle
Logomaker	Tareen et al.[47]	Pip V.0.8
Custom Code	In house	https://doi.org/10.5281/zenodo.19683785
Other		
MultiScreen$_{HTS}$-IP, 0.45 μm, transparent, sterile	Millipore	Cat# MSIPS4510
4D-Nucleofector™ Core Unit	Lonza	Cat#AAF-1002B
4D-Nucleofector™ X Unit	Lonza	Cat#AAF-1002X
Custom dCODE Dextramers®	Immudex	N/A
MR1 tetramers loaded 5-OP-RU	Prof. Dr. med. Jochen Mattner, University Hospital Erlangen, Germany	N/A

EXPERIMENTAL MODEL AND STUDY PARTICIPANT DETAILS

Study design

This was an exploratory study; therefore, a formal power analysis was not feasible. The sample size was predefined based on our experience and that of others in similar research contexts. The primary rationale of the study was to investigate the immunobiological mechanisms of adaptive immune responses following immunization, specifically with SARS-CoV-2 mRNA vaccines. No randomization or blinding was performed. The number of experimental replicates is indicated at the relevant sections of the manuscript. Blood samples from healthy donors who received a vaccination at the Vaccination and Travel Clinic of the University Hospital Erlangen were used as study material and served as the inclusion criterion. The following individuals were excluded from participation in this study: individuals unable to provide informed consent, minors, pregnant or breastfeeding individuals, and persons in a dependent relationship with other study participants or the study investigators.

Study cohort CoVa-Adapt

Ethics approval was granted by the local Ethics Committee of the Medical Faculty of the University Hospital of Erlangen, Friedrich-Alexander University Erlangen-Nürnberg, Germany (350_20B). Samples were collected after informed consent of the donors. Analyses from this cohort have been previously published[28,32,48] and the cohort (DRKS-ID: DRKS00034356) is described in detail in Table S1. HLA-typing was previously published.[28] In brief, donors were 23–58 years old (median: 42; interquartile range (IQR) 29–51), 55% female, of European Caucasian ethnicity, overall healthy (no chronic medication), of normal weight, and received a three-dose mRNA vaccination regimen with Comirnaty. Time intervals between immunizations were 22–28 days (median 23, IQR 23–25) between 1st and 2nd dose, and 196–244 days (median 227, IQR 216.5–229) between 2nd and 3rd dose. Blood was sampled before the 1st dose, 8–13 days post 1st dose (median 10, IQR 9–10), 9–11 days post 2nd dose (median 10, IQR 10–11), 195–211 days post 2nd dose (median 210, IQR 209–210), 9–12 days post 3rd dose (median 10, IQR 10-10) and 157–202 days post 3rd dose (median 189, IQR 189–190). Additional blood samples were collected for seven donors 101–126 days (median 108, IQR 108–113.5) after 3rd dose. Some donors experienced SARS-CoV-2 breakthrough infections after day 10 post 3rd dose which is indicated in the figures or figure legends if applicable. These breakthrough infections were self-reported and confirmed by PCR tests. 44% of breakthrough infections could be additionally validated by SARS-CoV-2 nucleocapsid^{+} serology, while no infection-free donor had detectable SARS-CoV-2 nucleocapsid-specific antibodies.

Peripheral blood mononuclear cell (PBMC) isolation

PBMCs were isolated from citrated peripheral blood by density gradient centrifugation using a BioColl density medium with a density of 1.077 g/mL (BioSell, BS.L 6115). Cells were resuspended in heat-inactivated FCS +10% DMSO and stored in liquid nitrogen.

METHOD DETAILS

Multiparametric flow cytometry for T cells

The following antibodies were used for T cell analysis: from BD Biosciences: anti-CD4-BUV395 (564724, 1:200), anti-CD19-PE/CF594 (562294, 1:200), anti-CD69-PerCP-Cy5.5 (560738,1:100), anti-IFNg-FITC (340449, 1:10), anti-IL-2-APC (341116, 1:20); from BioLegend: anti-CD4-BV510 (300545, 1:50), anti-CD8-APC (301049, 1:400), anti-human a/b TCR (hTCR)-FITC (306706, 1:200), anti-mouse TCR β chain (mTRBC)-APC/Fire750 (109246, 1:100), anti-CD45RA-PerCP-Cy5.5 (304121,1:400), anti-CD62L-PacificBlue (304825,1:400), anti-CD154-PerCP-Cy5.5 (310833, 1:100), anti-CD137-PE-Cy7 (309817, 1:100), anti-human TCR Va7.2-BV711 (351731, 1:50); from Thermo Fisher Scientific: anti-CD4-PE (12-0049-42, 1:400), anti-CD8-eF450 (48-0086-42, 1:200), anti-CD56-FITC (11-0566-42, 1:200), anti-CD45-PerCP-Cy5.5 (45-0459-42, 1:100), anti-CD45-PE/Cy7 (25-9459-42, 1:400); from Agilent Technologies: anti-CD45-PacificBlue (PB986, 1:50); from Miltenyi: anti-CD154-APC (130-113-603,1:100). For the viability staining, ethidium-monoazide-bromide (EMA; ThermoFisher, E1374), propidium iodide (PI; ThermoFisher, P1304MP), or ZombieNIR Fixable Viability Kit (BioLegend, 423106, 1:1000) was used.

Cells were first washed twice with cold FACS buffer (PBS +0.5% BSA). For experiments involving fixation and permeabilization, cells were resuspended in 100 μL of FACS buffer containing EMA (1:1000), incubated under bright light for 15 min, and washed once with cold FACS buffer before being incubated with 25 μL of surface antibody mix. In experiments without fixation/permeabilization, cells were directly resuspended in 25 μL of surface antibody mix and incubated on ice for 20 min. Surface staining was followed by two washes with cold FACS buffer if EMA staining had been performed, or one wash if not. In the latter case, cells were subsequently resuspended in 50 μL of FACS buffer containing PI (1:100), incubated for 3 min, and washed twice with cold FACS buffer. Where applicable, fixation and permeabilization were performed using the BD Cytofix/Cytoperm Kit (BD Biosciences, 554714) according to the manufacturer's instructions, followed by one wash with cold Perm/Wash buffer (1×) and one final wash with cold FACS buffer. Samples were acquired on a LSRFortessa Cell Analyzer (BD Biosciences) and analyzed with FlowJo 10.7.2 (Tree Star Inc.).

IFNg Enzyme-linked immunospot (ELISpot)

Cryopreserved PBMCs were thawed and rested overnight at 1×10^6 cells/mL in complete RPMI medium (cRPMI: RPMI 1640 Medium +10% heat-inactivated FCS, 0.05 mM β-mercaptoethanol, 0.05 mg/mL gentamicin, 1.1915 g/L HEPES, 0.2 g/L L-glutamine, 100 U/mL Penicillin-Streptomycin). ELISpot plates (Millipore, MSIPS4510) were coated with anti-human IFNg monoclonal antibody (clone 1-DIK, Mabtech, 3420-3-1000) at 0.5 μg/well overnight at 4°C. Plates were washed with sterile PBS and subsequently blocked with cRPMI medium for 1–2 h at 37°C. PBMCs were seeded at a density of 400,000 cells/well and stimulated with 11aa overlapping 15-mer PepMix SARS-CoV-2 spike glycoprotein peptide pool (JPT, PM-WCPV-S-2) or SARS-CoV-2 nucleoprotein peptide pool (JPT, PM-WCPV-NCAP-2) at a concentration of 1 μg/mL for 20 h at 37°C. For the unstimulated condition, PBMCs were cultured in cRPMI medium and respective dilution of solvent DMSO. As a positive control, PBMCs were stimulated with 25 ng/mL phorbol myristate acetate (PMA) (Sigma-Aldrich, P1585-1 mg) and 1 μg/mL ionomycin (Sigma-Aldrich, I9657-1 MG). The following steps were performed at room temperature. Plates were washed with PBS containing 0.05% Tween 20 (Sigma-Aldrich, P9416-50 mL) and incubated with biotinylated anti-human IFNγ monoclonal antibody (clone 7-B6-1, Mabtech, 3420-6-250) at 0.2 μg/well for 2 h. Plates were washed a second time with PBS containing 0.05% Tween 20 and subsequently incubated with an avidin-biotinylated peroxidase complex (VECTASTAIN Elite ABC-HRP Kit, Vector Laboratories, VEC-PK-6100) for 1–2 h. Afterward, plates

were washed first with PBS containing 0.05% Tween 20 following one washing step with PBS. Plates were developed by the addition of AEC substrate solution (Sigma-Aldrich, 152224-10 mL) for 15 min, washed with water and dried for 24 h in the dark. Analysis was performed on an ImmunoSpot Analyzer (Cellular Technologies Limited).

Reverse phenotyping

Single-cell RNA sequencing (scRNAseq) was performed for PBMCs from two CoVa-Adapt donors at a total of four time-points after primary (P), secondary (S), and tertiary (T) vaccination. Three independent experiments (Experiments 1–3) were conducted and pooled into a single dataset (Table S2). PBMCs were thawed from cryopreserved stocks and rested overnight at 1×10^6 cells/mL in cRPMI medium.

For each donor, 2×10^6 PBMCs were stimulated with stimulated with 11aa overlapping 15-mer PepMix SARS-CoV-2 spike glycoprotein peptide pool (JPT, PM-WCPV-S-2) at a concentration of 1 μg/mL for 4 h at 37°C. For the unstimulated condition, PBMCs were cultured in cRPMI medium and respective dilution of solvent DMSO. After stimulation, cells were washed with cold FACS buffer and stained with surface antibodies (anti-CD19-PE/CF594, anti-CD56-FITC, anti-CD8-APC, anti-CD4-PE, anti-CD62L-PacificBlue, anti-CD45RA-PerCP-Cy5.5). In Experiment 3, individual hashtag antibodies (2.5 μL per 5×10^6 PBMCs of TotalSeq-C anti-human hashtag antibodies 1–8, BioLegend, 394661, 394663, 394665, 394667, 394669, 394671, 394673, 394675) were included for sample multiplexing. All samples were incubated for 30 min on ice, followed by two washes with cold FACS buffer. Live/dead discrimination was performed using PI (1:200) immediately before sorting. Single, live, $CD19^-$and CD56-negative, $CD4^-$or CD8-positive, non-naïve (defined as CD45RA-positive and CD62L-negative, CD45RA-negative and CD62L-negative, or CD45RA-negative and CD62L-positive) lymphocytes were sorted in previously FCS-coated 96-well U-bottom plates filled with FACS buffer. In Experiment 3, eight different samples were pooled prior to sequencing and later distinguished using the unique TotalSeq-C hashtags during scRNAseq analysis. Cells were sorted on a FACS Aria II cell sorter (BD).

Immediately after sorting, cells were loaded to a Chromium Next GEM Chip K (10× Genomics) and Chromium Next GEM Single-Cell 5′ kits v.2 were used to generate GEX, VDJ and CITEseq libraries according to the manufacturer's instructions (10× Genomics, 1000263, 1000541, 1000252, 1000286, 1000250, 1000215, 1000190). Libraries were sent to Novogene (Cambridge, UK) and sequenced on an Illumina NovaSeq platform with PE150 strategy.

Dextramer staining

Single-cell RNA sequencing was performed for PBMCs from six CoVa-Adapt donors at a total of six time-points after primary (P), secondary (S), and tertiary (T) vaccination as well as for PBMCs from HIM 189 days after 215th vaccination (Table S3). PBMCs were thawed from cryopreserved stocks and rested overnight at 1×10^6 cells/mL in cRPMI medium.

For each donor, individual dextramer cocktails were prepared directly before staining (Table S3). For each cocktail, 1 μL per 5×10^6 cells of HLA-matched dCODE Dextramers (immudex) and 100 μM d-biotin (1/10 of total dextramer volume) were pre-mixed in FACS-buffer to block free binding sites. 5×10^6 PBMCs per donor and time-point were recovered and first stained with 50 μL of individual dextramer cocktails for 30 min on ice. Afterward, a cocktail of surface antibodies and viability staining (anti-CD19-PE/CF594, anti-CD56-FITC, anti-CD8-APC, anti-CD4-BV510, ZombieNIR), individual anti-CD45 antibodies (anti-CD45-PacificBlue, anti-CD45-PerCP/Cy5.5, anti-CD45-PE/Cy7), individual hashtag antibodies (2.5 μL per 5×10^6 PBMCs of TotalSeq-C anti-human hashtag antibodies 1–8, BioLegend, 394661, 394663, 394665, 394667, 394669, 394671, 394673, 394675), and TotalSeq-C antibodies (0.078 μg per 5×10^6 PBMCs anti-human CD45RA (BioLegend, 304163), 0.277 μg per 5×10^6 PBMCs anti-human CCR7 (BioLegend, 353251), 0.25 μg 5×10^6 PBMCs anti-human CXCR3 (BioLegend, 353747)) were added. For three samples, instead of individual TotalSeq-C antibodies, the TotalSeq-C Human Universal Cocktail, V1.0 (BioLegend, 399905) was added. On the day of the experiment, three vials of this universal cocktail were rehydrated in 18 μL of FACS buffer each, incubated for 5 min at room temperature, vortexed, and centrifuged at maximum speed for 30 s at room temperature. One vial was used to stain 5×10^6 PBMCs. Samples were incubated for an additional 30 min on ice. Cells were washed four times with cold FACS buffer and up to 8 samples were pooled prior to the sort. Pooled samples could be distinguished by individual CD45 color-barcoding at the sorter and by individual TotalSeq-C anti-human hashtag antibodies in the scRNAseq dataset. Single, live, $CD19^-$and CD56-negative, $CD4^-$or CD8-positive, dextramer-positive lymphocytes were sorted in previously FCS-coated 1.5 mL tubes filled with FACS buffer. Additionally, single, live, $CD19^-$and CD56-negative, total $CD4^-$or CD8-positive lymphocytes were sorted from three donors, as a framework for $CD4^-$and CD8-T-cell phenotypic clusters. Cells were sorted on a FACS Aria II cell sorter (BD).

Immediately after sorting, cells were loaded to a Chromium Next GEM Chip K (10× Genomics) and Chromium Next GEM Single-Cell 5′ kits v.2 were used to generate GEX, VDJ and CITEseq libraries according to the manufacturer's instructions (10× Genomics, 1000263, 1000541, 1000252, 1000286, 1000250, 1000215, 1000190). Libraries were sent to Novogene (Cambridge, UK) and sequenced on an Illumina NovaSeq platform with PE150 strategy.

Computational single-cell RNA sequencing data analysis

The Cellranger (version 6.0.2, 10× Genomics) "multi"-command was used to process the individual sequencing runs of the reverse phenotyping and the dextramer dataset using the references GRCh38 (version 2020A, 10× Genomics) and vdj-GRCh38 (version

5.0.0, 10× Genomics). For sequencing runs that include dextramers, CITE-markers, or hashtag antibodies, additional customized feature barcode references were used. The remaining analysis was performed using Scanpy (v.1.8.2[43]) and Scirpy (v.0.10.1[44]) following recent best practices.[49]

Quality control

GEX, antibody capture, and TCR data were fused on the run-level. Low-quality cells, such as doublets and dying cells, were filtered through thresholds on UMI counts, the number of detected genes, and the fraction of mitochondrial genes. Genes infrequently expressed in less than 10 cells were excluded. The gene expression count matrices were log1p-transformed after normalization to 10,000 counts per cell. Cells without TCR and outlier clusters were excluded from further analysis.

Annotation

Annotation was performed on a dataset level after fusing all runs from the reverse phenotyping and the dextramer dataset independently. Samples including hashtag antibodies were annotated for donor and time points via HashSolo,[45] and any annotated doublets or negative cells were removed. Cells with identical CDR3α and CDR3β amino acid sequences on primary or secondary chains were annotated as individual clonotypes, and clonal expansion was calculated per donor. For comparability, the IDs of clonotypes occurring in both datasets were unified. Scores of represented marker genes were calculated on a cell-level as described in their corresponding publication.[2,50] MAIT cells were annotated by the CDR3α sequence CAVMDSSYKLIF or by the combination of TRAJ33, TRAV1-2 together with TRBV20-1 or TRBV6 TCR genes. $CD4^+$, $CD8^+$, double-positive, and double-negative T cells were defined by the combination of corresponding marker genes CD4, CD8A, or CD8B at a threshold of 0.5. When protein surface markers were available, this was complemented by Hu.CD8 at 0.75 and Hu.CD4_RPA.T4 at 0.95. If not stated otherwise, only $CD4^+$ cells were considered for the analysis. In the reverse phenotyping dataset, γδ cells were defined at a γδ-marker score greater than 0 and not expressing a TCR. All cells with TCR and a γδ-score less than 0 were considered αβ cells. Leiden clustering[51] (resolutions: $r_{RP\_full}=0.75$, $r_{RP\_CD4}=1.25$, $r_{RP\_unstim}=0.75$, $r_{Dex\_CD4}=0.8$) and UMAP visualisation[52] ($n_{neighbors}=15$) were performed on the 5,000 most variable genes without TCR-forming genes on various subsets of the datasets.

Reactivity and specificity

In the reverse phenotyping dataset, the reactive cluster was indicated by *IFNG* expressed in more than 30% and a proliferation score greater 0.5 in more than 80% of cells, as well as a high fraction of stimulated cells. All cells of a reactive clonotype with at least one member in the reactive cluster were marked as reactive. In the dextramer dataset, specificity toward TFEYVSQPFLMDLE was assigned for cells with a UMI count of 6 or higher. Additionally, the counts for TFEYVSQPFLMDLE were required to amount to at least 40% of total UMIs, and 50% of the clonotype members must have expressed specificity.

Analysis

Differential expression analysis of genes and surface proteins was performed via ''scanpy.tl.rank_genes_groups'' through a *t*-test with Benjamini-Hochberg correction. To obtain the TCR similarity network (Figure 3H), the reverse phenotyping dataset and the dextramer dataset were combined with annotated TCR data from Pogorelyy et al.[33] TCR clonotypes were clustered using TCRdist3 as a distance measure.[36] Connected components of clonotypes within 120 TCRdist units were formed, and visualized through the ''Circle Pack Layout'' in Gephi (v.0.9.7[53]) with component ID and modularity as hierarchy. CDR3 motifs were calculated on the respective amino acid sequence aligned by MUSCLE[46] and visualized through Logomaker.[47]

Cell numbers of all sequencing runs and sub-samples are available in Table S7.

Transgenic TCR re-expression in primary human T cells

A coherent description for the workflow of targeted TCR re-expression in primary human T cells using CRISPR-Cas9-mediated orthotopic TCR replacement has previously been published.[28,54,55] A brief description including all relevant alterations to the published protocol is summarized in the following chapters ''Transgenic TCR DNA template design'', ''Double-stranded DNA production'', ''T cell activation for genetic editing'', ''Ribonucleoprotein production'', and ''Orthotopic TCR replacement (OTR)''.

Transgenic TCR DNA template design

The DNA template was designed *in silico* and synthesized by Twist Bioscience. The construct had the following structure: The left homology arm (LHA; 396 bp) was followed by a self-cleaving peptide P2A and the TCR β-chain which consisted of the human variable part (VDJβ) and the murine TCR β constant region with an additional cysteine bridge (mTRBC-Cys).[56] The subsequent self-cleaving peptide T2A separated the β-chain from the following a-chain which was designed according to the same principle with the human variable part (VJa) being followed by the murine TCR α constant region with an additional cysteine bridge (mTRAC-Cys).[56] After the stop codon (TGA) and the bovine growth hormone polyA signal (bGHpA), the 330 bp right homology arm (RHA) concluded the HDR template. For sequences of these segments see Tables S8 and S9.

Double-stranded DNA production

The DNA construct was ordered as a sequence-verified plasmid gene via a commercial provider (Twist Bioscience). The lyophilized plasmid was reconstituted with sterile water to 60 ng/μL and amplified by PCR to generate a linearized double-stranded HDR template. A truncated Cas9 Target Sequences (CTS) was incorporated at the 5′-end of the HDR template by the genomic primer targeting the hTRAC LHA. Each 100 μL PCR reaction contained 1 x Herculase II Reaction Buffer, 0.4 μM hTRAC HDR genomic forward primer targeting LHA (5′-TCTCTCTCTCAGCTGGTACACGGCTGCCTTTACTCTGCCAGAG-3′), 0.4 μM hTRAC HDR genomic reverse primer

targeting RHA (5′-CATCATTGACCAGAGCTCTG-3′), 0.5 mM dNTPs, 1 μL Herculase II Fusion DNA Polymerase, and 60 ng reconstituted DNA in PCR grade water. The PCR was run with the following cycling conditions: Initial denaturation at 95°C for 3 min, 34 cycles of 95°C for 30 s, 63°C for 30 s and 72°C for 3 min, final elongation at 72°C for 3 min, and hold at 4°C. Successful amplification was confirmed with an 1% agarose gel and amplified HDR template was purified with a MinElute PCR Purification Kit (Qiagen, 28004) according to the manufacturer's instructions.

T cell activation for genetic editing

PBMCs were isolated from blood provided by healthy volunteers (Transfusion Medicine, University Hospital Erlangen) and frozen at −80°C for storage. Ethics approval was granted by the local Ethics Committee of the Medical Faculty of the University Hospital of Erlangen, Friedrich-Alexander University Erlangen-Nürnberg, Germany (392_20Bc). Samples were collected after informed consent of the donors. For T cell activation, these PBMCs were thawed and overnight-rested at 2×10^6 cells/mL in cRPMI medium supplemented with 50 U/mL Interleukin-2 (IL 2). Afterward, PBMCs were activated for two days at 1×10^6 cells/mL on tissue-culture flasks with 1 μg/mL of surface-bound anti-CD3 (BioLegend, 317302) and anti-CD28-antibodies (BioLegend, 302902) in medium supplemented with 300 U/mL IL 2 (Peprotech, 200-02), 5 ng/mL Interleukin-7 (Peprotech, 200-07), and 5 ng/mL Interleukin-15 (Peprotech, 200-15).

Ribonucleoprotein production

Activated PBMCs were electroporated with ribonucleoproteins (RNPs) targeting the endogenous *hTRAC* and *hTRBC* locus as well as the purified HDR template. For final electroporation, 3.5 μL of *hTRAC* and 3 μL of *hTRBC* RNP (final concentration 20 μM) were required per electroporation sample. First, 40 μM gRNAs were produced by mixing equimolar amounts of *trans*-activating crRNA (tracrRNA) (Integrated DNA Technologies, 1072534) with *hTRAC*[57] crRNA (5′-AGAGTCTCTCAGCTGGTACA-3′, Integrated DNA Technologies) or *hTRBC* crRNA[54] (5′-GGAGAATGACGAGTGGACCC-3′, Integrated DNA Technologies) and incubating the mixtures at 95°C for 5 min with subsequent cool down to room temperature. Afterward, 50 μg/sample poly-L-glutamic acid (PGA; Sigma-Aldrich, P4761) were added to *hTRAC* gRNA[58,59] and 20 μM electroporation enhancer (Integrated DNA Technologies, 10007805) were added to both *hTRAC* and *hTRBC* gRNA. RNP production was concluded by adding equal volume of Cas9 Nuclease V3 (Integrated DNA Technologies, 1081059, diluted to 6 μM) to *hTRAC* and *hTRBC* gRNA (40 μM) respectively. RNPs were incubated for 15 min at RT and subsequently stored on ice for processing at the same day. For the calculations above, the volume of PGA was not considered.

Orthotopic TCR replacement (OTR)

Prior to electroporation, DNA-sensing inhibitors RU.521 (small-molecule inhibitor of cyclic GMP-AMP synthase (cGAS); InvivoGen, inh-ru521)[58] was added to the cells at a final concentration of 4.82 nM for 6 h. Afterward, activation was stopped by transferring cells to a new plate in fresh cRPMI medium. For electroporation, 1×10^6 activated cells per electroporation sample were resuspended in 20 μL P3 electroporation buffer (Lonza, V4SP-3960) and then mixed with DNA/RNP mix (0.5 μg HDR template, 3.5 μL *hTRAC* and 3 μL *hTRBC* RNPs). After transfer into the 16-well Nucleocuvette Strip (Lonza, V4SP-3960), cells were electroporated (pulse sequence EH100) in the Lonza 4D-Nucleofector. After electroporation, cells were rescued in 900 μL of antibiotic-free RPMI medium supplemented with 180 U/mL IL-2. After 15 min, 100 μL of a mixture containing 0.5 μM HDAC class I/II Inhibitor Trichostatin A (AbMole, M1753) and 10 μM DNA-dependent protein kinase (DNA-PK) inhibitor M3814 (chemietek, CT-M3814) was added to each sample.[60] Cells were incubated for 12–18 h in a 24-well plate, before the medium was supplemented with an antibiotic mix containing gentamicin, penicillin and streptomycin to produce cRPMI medium. 24 h after electroporation, cells were transferred into a new 24-well plate and cultivated in a final volume of 1 mL fresh cRPMI medium supplemented with 180 U/mL IL-2. Four days after electroporation, successful editing was validated by flow cytometry (anti-CD4-PE, anti-CD8-eF450, anti-human a/b TCR (hTCR)-FITC, anti-mouse TCR β chain (mTRBC)-APC/Fire750). Cells were cultivated for additional seven to eight days in cRPMI with addition of 50 U/mL IL-2 every two days before specificity was determined by peptide-induced activation marker expression.

Peptide-pulsing of autologous PBMCs

To assess the reactivity of TCR-engineered T cells against SARS-CoV-2 spike epitopes, TCR-engineered T cells were co-cultured with peptide-pulsed autologous PBMCs. Autologous PBMCs were isolated and cryopreserved in liquid nitrogen as described above. One day prior to the experiment, PBMCs were thawed and rested overnight at 1×10^6 cells/mL in cRPMI. For peptide pulsing, 1×10^6 PBMCs per condition were incubated with 1 μg/mL of an 11aa overlapping 15-mer PepMix SARS-CoV-2 spike glycoprotein peptide pool or 10^{-4} M of NQKLIANQF peptide for 2 h at 37°C. After incubation, excess peptide was removed by washing. As a negative control, PBMCs were treated with an equivalent dilution of DMSO, the solvent used for the peptide pool.

Peptide-induced activation marker expression by TCR-engineered T cells

The percentage of transgenic TCR (mTRBC)+ cells within the TCR-engineered T cell population was determined by flow cytometry one day prior to co-culture. A total of 2×10^4 transgenic TCR (mTRBC)+ T cells were co-cultured with 2×10^4 peptide-pulsed autologous PBMCs for 4 h at 37°C in cRPMI, in the presence of 1 μg/mL anti-CD40 blocking antibody (Miltenyi Biotec, 130-094-133). As a positive control, TCR-engineered T cells were stimulated with 25 ng/mL PMA (Sigma-Aldrich, P1585-1 mg) and 1 μg/mL ionomycin

(Sigma-Aldrich, I9657-1 MG). Following co-culture, cells were first stained with EMA, followed by surface staining (anti-CD4-BUV395, anti-CD8-eF450, anti-CD19-PE/CF594, anti-human TCR a/b-FITC, anti-human TCR a/b-APC/Fire750, anti-CD154-APC, anti-CD69-PerCP-Cy5.5), then fixed. In the case of MAIT TCR clone 14370, cells were first stained with EMA, followed by surface staining (anti-CD4-BUV395, anti-CD8-eF450, anti-CD19-PE/CF594, anti-human TCR a/b-FITC, anti-human TCR a/b-APC/Fire750, anti-human TCR Va7.2-BV711), fixation and intracellular staining (anti-IFNg-FITC, anti-IL-2-APC, anti-CD154-PerCP-Cy5.5, anti-CD137-PE-Cy7). Samples were acquired on a LSRFortessa Cell Analyzer (BD Biosciences) and analyzed with FlowJo 10.7.2 (Tree Star Inc.).

MR1 tetramer staining

MR1 tetramers loaded with the MAIT cell ligand 5-OP-RU were kindly provided by Prof. Dr. med. Jochen Mattner (University Hospital Erlangen). TCR-engineered T cells were washed twice with cold FACS buffer prior to staining. Subsequently, 25 μL of MR1 tetramers were added to each sample, and cells were incubated for 40 min at room temperature in the dark. After staining, cells were centrifuged at 480 × *g* for 5 min, and the supernatant was discarded. Cells were then stained with EMA, followed by surface staining (anti-CD4-BUV395, anti-CD8-eF450, anti-CD19-PE/CF594, anti-human TCR a/b-FITC, anti-human TCR a/b-APC/Fire750, anti-human TCR Va7.2-BV711). Samples were acquired on a LSRFortessa Cell Analyzer (BD Biosciences) and analyzed with FlowJo 10.7.2 (Tree Star Inc.).

QUANTIFICATION AND STATISTICAL ANALYSIS

Statistical analyses were performed as appropriate for each individual experiment and type of data. Specific details regarding the statistical methods used are provided in the corresponding figure legends and relevant methods section.